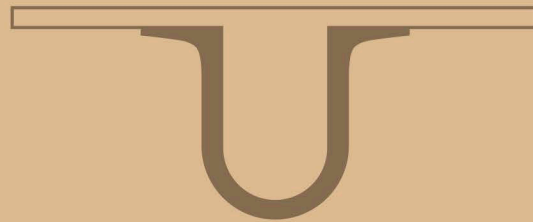




UNIVERSIDADE D  
COIMBRA



Tomás Périé de Barros

TIME-DEPENDENT LOCAL DENSITY OF STATES  
AS A TOOL TO STUDY OPTICAL RESPONSE

Dissertação no âmbito do Mestrado em Física, com especialização em Física da Matéria Condensada,  
orientada pelo Professor Doutor Fernando Manuel da Silva Nogueira  
e apresentada ao Departamento de Física da Faculdade de Ciências e Tecnologia  
da Universidade de Coimbra

Outubro de 2018





Universidade de Coimbra  
Faculdade de Ciências e Tecnologia  
Departamento de Física

# Time-dependent local density of states as a tool to study optical response

Tomás Barros

Advisor  
Dr. Fernando Nogueira

Submitted in part fulfillment of the requirements for the degree of  
Master in Physics  
September 2018



## **Acknowledgements**

I would like to thank my advisor Dr. Fernando Nogueira for his guidance and help on all the problems along the way. I would also like to thank all my friends and colleagues for their support and advice throughout the years.

Lastly I would like to thank my family, whose hard work allowed me to be here, for all their support, help and love.



## Abstract

Photosynthesis is one the most important reactions that exist. However it is not yet completely understood. Although many steps of this important process are already known, a fundamental piece is still not 100% clear: the energy transfer mechanism between photoreceptors in, e.g., green plants. The Förster[1] mechanism is assumed to be the dominant non-radiative energy transfer process, but the available theoretical and experimental tools are not enough to clarify this matter without doubt. The analysis of the local density of states is one tool that may prove insightful in the study of energy transfer mechanisms in light harvesting complexes. This thesis focuses on the implementation of the calculation of the time dependent density of states in Bader regions in the Octopus code.





## Resumo

A fotossíntese é uma das mais importantes reações químicas que existem não sendo no entanto completamente compreendida. Apesar de muitos dos passos deste importante processo serem já conhecidos uma parte não é ainda 100% clara: o mecanismo de transferência de energia entre fotorreceptores em, por exemplo, plantas verdes. Assume-se que o mecanismo de Förster[1] é o processo não radiativo de transferência de energia dominante, não sendo no entanto as ferramentas teóricas e experimentais disponíveis suficientes para clarificar esta matéria. A análise da densidade local de estados é uma ferramenta que pode vir a provar-se útil no entendimento do mecanismo de transferência de energia em complexos de captação de luz. Esta tese foca-se na implementação do cálculo da densidade local de estados dependente do tempo em regiões de Bader feita no código Octopus.



# Contents

<b>Acknowledgements</b>	<b>i</b>
<b>Abstract</b>	<b>iii</b>
<b>Resumo</b>	<b>v</b>
<b>1 Introduction</b>	<b>1</b>
1.1 Motivation and Objectives . . . . .	1
1.2 Synopsis . . . . .	2
<b>2 Background Theory</b>	<b>3</b>
2.1 Introduction . . . . .	3
2.2 Density Functional Theory . . . . .	3
2.2.1 Hohenberg-Kohn Theorems . . . . .	4
2.2.2 The Kohn-Sham equations . . . . .	5
2.2.3 Local-Density Approximation . . . . .	6
2.2.4 Time-Dependent Density Functional Theory . . . . .	7
2.3 Bader Volumes . . . . .	10

2.4	Local Density of States . . . . .	15
<b>3</b>	<b>Results</b>	<b>17</b>
3.1	Introduction . . . . .	17
3.2	Implementation of the Bader Volumes . . . . .	17
3.3	Calculation of the local density of states . . . . .	22
<b>4</b>	<b>Conclusion and Future work</b>	<b>39</b>
4.1	Conclusion . . . . .	39
4.2	Future Work . . . . .	39
	<b>Bibliography</b>	<b>40</b>
<b>A</b>	<b>Demonstration of the first Hohenberg-Kohn theorem</b>	<b>43</b>
<b>B</b>	<b>Local density of states in the betaine molecule for the remaining iterations.</b>	<b>45</b>

# List of Tables

3.1	Properties calculated on each Bader regions on a N <sub>2</sub> molecule. . . . .	21
3.2	Properties calculated on each Bader regions on a methane molecule. . . . .	22
3.3	Parameters for the laser envelope function. . . . .	24
3.4	Parameters for the laser envelope function in the nitroaniline case. . . . .	32



# List of Figures

2.1	Schematic representation of the Runge-Gross Theorem. . . . .	9
2.2	Gradient paths for the plane containing the nuclei in $C_2H_4$ . . . . .	11
2.3	Representation of the boron atom in $BH_3$ . . . . .	13
2.4	Example of the bifurcation mechanism. . . . .	14
2.5	Example of the conflict mechanism. . . . .	15
2.6	Density of states for the 3D homogeneous electron gas. . . . .	16
3.1	Illustration of the algorithm used to find the Bader Regions . . . . .	19
3.2	Bader regions on a $N_2$ molecule. . . . .	20
3.3	Bader regions on a methane molecule. . . . .	21
3.4	3D configuration of the betaine molecule. . . . .	23
3.5	Scheme of the partition of the betaine molecule into two larger regions. . . . .	24
3.6	Local density of states for the betaine molecule. . . . .	25
3.7	Laser field used to excite the betaine molecule. . . . .	26
3.8	Absorption spectrum for the betaine molecule. . . . .	26
3.9	Time-dependent local density of states for the betaine molecule in iteration 1000. . . . .	27

---

3.10	Time-dependent local density of states for the betaine molecule in iteration 1500.	28
3.11	Time-dependent local density of states for the betaine molecule in iteration 3000.	29
3.12	Change in population in each of the betaine regions in time. . . . .	30
3.13	3D configuration of the nitroaniline molecule. . . . .	30
3.14	Scheme of the partition of the nitroaniline molecule into two larger regions. . . .	31
3.15	Local density of states for the nitroaniline molecule. . . . .	33
3.16	Laser field used to excite the nitroaniline molecule. . . . .	34
3.17	Absorption spectrum for the nitroaniline molecule. . . . .	34
3.18	Time-dependent local density of states for the nitroaniline molecule in iteration 400. . . . .	35
3.19	Time-dependent local density of states for the nitroaniline molecule in iteration 800. . . . .	36
3.20	Time-dependent local density of states for the nitroaniline molecule in iteration 1400. . . . .	37
3.21	Change in population in each of the nitroaniline regions in time. . . . .	38
B.1	Time-dependent local density of states for the betaine molecule in iteration 250.	46
B.2	Time-dependent local density of states for the betaine molecule in iteration 500.	47
B.3	Time-dependent local density of states for the betaine molecule in iteration 750.	48
B.4	Time-dependent local density of states for the betaine molecule in iteration 1250.	49
B.5	Time-dependent local density of states for the betaine molecule in iteration 1750.	50
B.6	Time-dependent local density of states for the betaine molecule in iteration 2000.	51
B.7	Time-dependent local density of states for the betaine molecule in iteration 2250.	52



B.8	Time-dependent local density of states for the betaine molecule in iteration 2500.	53
B.9	Time-dependent local density of states for the betaine molecule in iteration 2750.	54
B.10	Time-dependent local density of states for the betaine molecule in iteration 3250.	55
B.11	Time-dependent local density of states for the betaine molecule in iteration 3500.	56
B.12	Time-dependent local density of states for the betaine molecule in iteration 3750.	57
B.13	Time-dependent local density of states for the betaine molecule in iteration 4000.	58
B.14	Time-dependent local density of states for the betaine molecule in iteration 4250.	59
B.15	Time-dependent local density of states for the betaine molecule in iteration 4500.	60
B.16	Time-dependent local density of states for the betaine molecule in iteration 4750.	61
B.17	Time-dependent local density of states for the betaine molecule in iteration 5000.	62
B.18	Time-dependent local density of states for the betaine molecule in iteration 5250.	63
B.19	Time-dependent local density of states for the betaine molecule in iteration 5500.	64
B.20	Time-dependent local density of states for the betaine molecule in iteration 5750.	65
B.21	Time-dependent local density of states for the betaine molecule in iteration 6000.	66



# Chapter 1

## Introduction

### 1.1 Motivation and Objectives

Photosynthesis is one of the most interesting and highly studied biochemical processes, not only for its central importance in the development and sustainability of life on Earth but also for the myriad of technological innovations that a detailed understanding of it might lead to, from crop production optimization[2] to better ways of converting sunlight into usable energy[3].

Despite that the process through which the transfer of energy between successive chlorophylls occurs remains elusive. Existing theories, such as Förster's resonance energy transfer, are not totally satisfactory [1]. Advancements in computational resources and algorithm optimization have made possible the simulation, based on first-principles, of the light harvesting complexes where photosynthesis happens [4]. These studies aim to find some better insight on how the energy transfer occurs. The analysis of the time-dependent local density of states stands as another option in the bag of tools to tackle this problem.

The aim of the work in this thesis was to implement the time-dependent local density of states in the real-space time-dependent density functional theory code Octopus [5], so that studies like this, and possibly other ones, can then be carried out.

## 1.2 Synopsis

This thesis is divided into four parts, the first, and present one, being an introductory chapter.

The second chapter presents some concepts and theories needed for the execution of this thesis.

There are three distinct aspects to be discussed, each in its own sub-chapter. The first one briefly explains Density Functional Theory (DFT), the backbone of all calculations done on the Octopus code, from the theorems that spurred its development to Time Dependent Density Functional Theory (TDDFT), an extension to DFT that allows the study of time-dependent phenomena. The second one deals with how to divide different molecules into smaller regions that make physical sense, as proposed in Richard Bader's theory of atoms in molecules. Lastly the third one introduces the concept of density of states, the central property of this work.

The third chapter shows the work developed, illustrating how the space is partitioned and the local density of states calculated.

Finally, in the fourth chapter, the conclusions of this thesis are given, as well as suggestions for future work.

# Chapter 2

## Background Theory

### 2.1 Introduction

In this chapter a brief overview of the most important theoretical concepts that form the basis for the work developed in this thesis is given. First we give a small explanation of DFT, the theory that forms the basis for the octopus code. Secondly the theory of atoms in molecules, used here to divide the space into different regions where to calculate the density of states, is discussed. Finally we talk about the density of states, the property whose calculation is the aim of this work.

### 2.2 Density Functional Theory

The problem of electronic structure is an exceedingly complex one. The Hamiltonian for a  $N$  electron and  $M$  nuclei system is:

$$H_{tot}(\vec{r}_1, \dots, \vec{r}_N, \vec{R}_1, \dots, \vec{R}_M) = - \sum_{i=1}^N \frac{1}{2} \nabla_i^2 - \sum_{I=1}^M \frac{1}{2M_I} \nabla_I^2 - \sum_{i=1}^N \sum_{I=1}^M \frac{Z_I}{|\vec{r}_i - \vec{R}_I|} + \sum_{i=1}^N \sum_{j>i}^N \frac{1}{|\vec{r}_i - \vec{r}_j|} + \sum_{I=1}^M \sum_{J>I}^M \frac{Z_I Z_J}{|\vec{R}_I - \vec{R}_J|} \quad (2.1)$$

where  $\vec{r}_i$  and  $\vec{R}_I$  are, respectively, the position of electron  $i$  and the position of nucleus  $I$ ,  $Z_I$  is the atomic number of nucleus  $I$  and  $M_I$  is the ratio between its mass and the electron mass. Atomic units ( $e^2 = \hbar = m_e = 1$ ) are used here and throughout the text. The different terms on the right hand side represent, from the first to the last one, the kinetic energy of the electrons, the kinetic energy of the nuclei, the Coulombic attraction between electron and nuclei, the repulsion between electrons and the repulsion between nuclei.

Solving the Schrodinger equation for this Hamiltonian is not feasible. The sheer number of bodies in play makes it computationally intractable. To simplify this problem several approximations are used. One of them is the Born–Oppenheimer approximation. In this approximation the motion of the nuclei and the electrons can be separated. Because the nuclei are a lot heavier than the electrons we assume the electrons move in a field created by the static nuclei. This allows the separation of the original problem into two, the nuclear part and the electronic part. Although this greatly reduces the problem the number of variables is still great enough that the electronic problem alone is not solvable unless other approaches are used.

One way to do this is by using density functional theory (DFT), the main idea behind it being that all information regarding the system is contained in the ground-state electronic density of the whole system:

$$\rho(\vec{r}) = N \int d\vec{r}_2 \dots d\vec{r}_N |\Psi_0(\vec{r}, \vec{r}_2 \dots \vec{r}_N)|^2 \quad (2.2)$$

More specifically this means that any property of the system can be written as a functional of the many-body electron density, hence the name of the theory. This greatly simplifies the problem as we no longer need to know  $\Psi_0(\vec{r}, \vec{r}_2 \dots \vec{r}_N)$ , which is a function of  $3N$  variables, we only need to know  $\rho(\vec{r})$ , which has just three variables. This was made possible by two theorems known as the Hohenberg-Kohn theorems.

### 2.2.1 Hohenberg-Kohn Theorems

These two theorems were first proven by Hohenberg and Kohn in 1964 [6].

The first Hohenberg-Kohn theorem says that the external potential  $v_{ext}(\vec{r})$  is uniquely determined, within a trivial additive constant, by the electron density. This means that the external potential is a unique functional of the density. For proof of this theorem see appendix A.

If the potential is determined by the density then so is the Hamiltonian and therefore also the wave-functions. Consequently the expectation value of any observable is also a functional of  $\rho$ , which constitutes the basis of DFT:

$$O[\rho] = \langle \Psi[\rho] | \hat{O} | \Psi[\rho] \rangle \quad (2.3)$$

The second Hohenberg-Kohn theorem states that the energy of the system can be written as a functional of the density, valid for any  $v_{ext}(\vec{r})$ :

$$E_{HK}[\rho] = F[\rho] + \int v_{ext}(\vec{r})\rho(\vec{r})d(\vec{r}) \quad (2.4)$$

where  $F[\rho]$  is a universal functional encompassing all interactions not dependent on the external potential and therefore valid for any number of electrons. The theorem states that the exact ground state energy is the minimum of this energy functional, that can be found using, for example, the variational principle.

### 2.2.2 The Kohn-Sham equations

One of the most used approaches in DFT, and the one used in Octopus, is the Kohn-Sham formulation. The big advantage of this approach is simplifying the  $N$  electron problem by instead solving a fictitious system of non-interacting particles that generate the same density as the original system. Given that the density determines in an unequivocal way all the properties of the system, if a non-interacting system has the same density as the real system, the real problem can be solved through the non-interacting system. The new equations are the Kohn-Sham equations [7]:

$$\left[ -\frac{1}{2}\nabla^2 + v_{KS}(\vec{r}) \right] \phi_i(\vec{r}) = \epsilon_i \phi_i(\vec{r}) \quad (2.5)$$

with the ground state density given by

$$\rho(\vec{r}) = \sum_{i=1}^N |\phi_i(\vec{r})|^2 \quad (2.6)$$

The effective potential for the independent particles, known as the Kohn-Sham potential is:

$$v_{KS}(\vec{r}) = v_{ext}(\vec{r}) + v_{xc}(\vec{r}) + \int \frac{\rho(\vec{r}')}{|\vec{r} - \vec{r}'|} d\vec{r}' \quad (2.7)$$

where  $v_{xc}(\vec{r})$  is the exchange-correlation potential given by:

$$v_{xc}(\vec{r}) = \frac{\delta E_{xc}[\rho]}{\delta \rho(\vec{r})} \quad (2.8)$$

$E_{xc}$  is the exchange-correlation energy, a term that includes all non-trivial many-body contributions to the total energy of the system.

Given the functional dependency of the Kohn-Sham potential on the density, equations (2.5) and (2.6) can be used iteratively to find the ground state density of the system. This is done by starting with a guess density, calculating the corresponding potential, solving the KS equations for this new potential to find a new density, and repeating the whole process until self-consistency is achieved.

The only real unknown in this process is the exchange-correlation term, which has to be approximated. There are numerous approximations of this term, the most famous of them being perhaps the *local-density approximation*.

### 2.2.3 Local-Density Approximation

The local-density approximation (LDA) is the simplest way to approximate the exchange-correlation term. In this approximation the exchange-correlation energy at each point is simply



what it would be for an homogeneous electron gas of the same density, *i.e.*

$$E_{xc}^{HEG} = \int \epsilon_{xc}(\rho(\vec{r}))\rho(\vec{r})d\vec{r} \quad (2.9)$$

where  $\epsilon_{xc}$  is the exchange-correlation energy per particle of an uniform electron gas of density  $\rho$ . This value has been tabulated for many different densities using Monte Carlo methods by Ceperley and Alder [8].

This simple approximation is exact only for slowly-varying densities, which is not the case in real systems. However LDA turns out to be remarkably accurate for a wide variety of cases and not only useful but also hard to improve upon [9].

LDA, while the simplest, is far from the only approximation used. Other alternatives include generalized gradient approximations (GGA) [10], involving not only the density but also its gradient, meta-GGA, involving also the second derivative of the electron density [11], as well as more complex hybrid approaches [12].

## 2.2.4 Time-Dependent Density Functional Theory

So far we have only treated the system in its ground state. To study time-dependent problems we need to solve the time-dependent Schrodinger equation for an  $N$  electron wavefunction  $\Psi(\vec{r}_1, \dots, \vec{r}_N, t)$ :

$$H(\vec{r}_1, \dots, \vec{r}_N, t)\Psi(\vec{r}_1, \dots, \vec{r}_N, t) = i\frac{\partial}{\partial t}\Psi(\vec{r}_1, \dots, \vec{r}_N, t) \quad (2.10)$$

where the Hamiltonian is:

$$H(\vec{r}_1, \dots, \vec{r}_N, t) = -\sum_{i=1}^N \frac{1}{2}\nabla_i^2 + \sum_{i=1}^N v_{ext}(\vec{r}_i, t) + \sum_{i=1}^N \sum_{j>i}^N \frac{1}{|\vec{r}_i - \vec{r}_j|} + E_{nn}. \quad (2.11)$$

This is the generic version of Hamiltonian 2.1 where, because we are using the Born-Oppenheimer approximation, the kinetic energy of the nuclei is disregarded and their interaction with each other is considered as a constant,  $E_{nn}$ . The time dependency is on  $v_{ext}(\vec{r}_i, t)$  which includes the

nuclear field as well as any other external field, such as the one created by a laser.

To study the dynamics of the system we need to extend DFT to work with time-dependent external potentials. The first step is to find a time-dependent analogue of the Hohenberg-Kohn theorem. This is known as the Runge-Gross theorem [13].

This theorem establishes the existence of a one-to-one mapping between the time-dependent potential  $v_{ext}(\vec{r}, t)$  and the time-dependent density

$$\rho(\vec{r}, t) = N \int d\vec{r}_2 \dots d\vec{r}_N |\Psi(\vec{r}, \vec{r}_2 \dots \vec{r}_N, t)|^2, \quad (2.12)$$

evolving from a fixed initial state  $\Psi_0$ . That is, we can write the external time-dependent potential as a functional of the time-dependent density. The potential is determined up to a purely time-dependent constant which in turn means the wave-function is determined up to a purely-time-dependent phase  $\alpha(t)$ , so that we can see this wave-function as a functional of the density and the initial state:

$$\Psi(t) = e^{-i\alpha(t)} \Psi[\rho, \Psi_0](t) \quad (2.13)$$

This then means the expectation value of any observable  $\hat{O}(t)$  is also a functional of the density and the initial state:

$$O[\rho, \Psi_0] = \langle \Psi[\rho, \Psi_0](t) | \hat{O}(t) | \Psi[\rho, \Psi_0](t) \rangle \quad (2.14)$$

A schematic representation of this loop is presented in figure 2.1.

This means that, for a given initial state, we only need to know a function of three spatial variables and time, the electronic density, in order to determine all properties of the system.

Now the only thing left in order to achieve a time-dependent version of DFT is to find a time-dependent version of the Kohn-Sham equations. The idea is the same as in the ground state case, substitute the real system with a system of non-interacting particles whose density, given by:

$$\rho(\vec{r}, t) = \sum_{i=1}^N |\phi_i(\vec{r}, t)|^2, \quad (2.15)$$

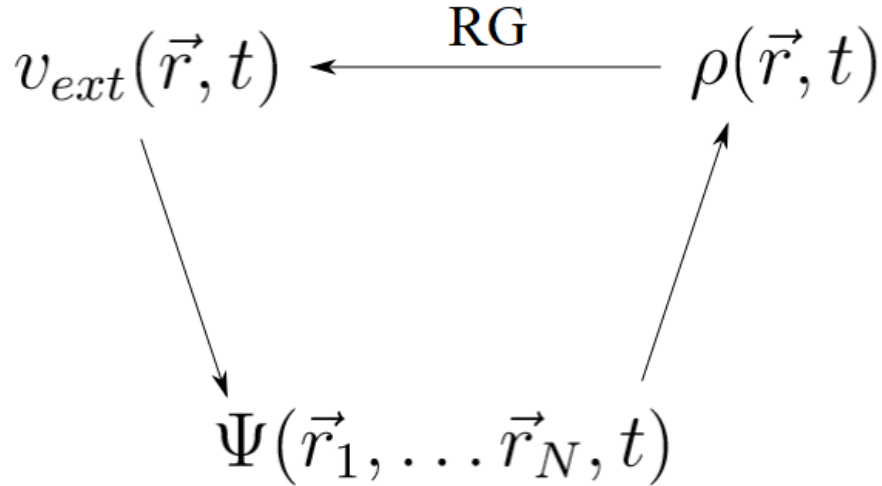


Figure 2.1: Schematic representation of the Runge-Gross Theorem. By solving the time-dependent Schrodinger equation the external potential  $v_{ext}(\vec{r}, t)$  determines the time-dependent wavefunction  $\Psi(\vec{r}_1, \dots, \vec{r}_N, t)$  which in turn determines the electronic density  $\rho(\vec{r}, t)$ . The Runge-Gross theorem closes the circle by providing a correspondence between the electronic density and the external potential.

is the same as that of the original interacting system for all time. This non-interacting system obeys the time-dependent Kohn-Sham equations:

$$\left[ -\frac{1}{2}\nabla^2 + v_{KS}(\vec{r}, t) \right] \phi_i(\vec{r}, t) = i\frac{\partial}{\partial t}\phi_i(\vec{r}, t) \quad (2.16)$$

The main problem in this approach is again finding the Kohn-Sham potential, which is again divided in three parts:

$$v_{KS}[\rho, \Phi_0](\vec{r}, t) = v_{ext}[\rho, \Psi_0](\vec{r}, t) + v_{xc}[\rho, \Psi_0, \Phi_0](\vec{r}, t) + \int \frac{\rho(\vec{r}', t)}{|\vec{r} - \vec{r}'|} d\vec{r}' \quad (2.17)$$

The first term is the external time-dependent potential, the last term is the time-dependent Hartree potential, that describes the interaction between the classical electronic charge distributions, and  $v_{xc}[\rho, \Psi_0, \Phi_0](\vec{r}, t)$  is the exchange-correlation potential where  $\Phi_0$  is the initial state of the non-interacting system. The choice of this initial state and the fact that the Kohn-Sham potential depends on it are exclusive to TDDFT and don't have a ground state analogue [14].

The great difficulty in the Kohn-Sham scheme is once more the exchange-correlation potential which again must be approximated. One useful procedure is to use adiabatic approximations, that is, we evaluate the functional at each time with the density  $\rho(\vec{r}, t)$ , thus constructing a functional that is local in time. The simplest of these is the adiabatic local density approximation (ALDA):

$$v_{xc}^{ALDA}(\vec{r}, t) = v_{xc}^{HEG}(\rho)|_{\rho=\rho(\vec{r},t)} \quad (2.18)$$

This approximation is valid for systems that vary slowly both in time and in space, which is generally not the case, but turns out to give very reasonable results for most, but not all, cases [14].

## 2.3 Bader Volumes

In order to calculate local properties in a molecule one needs to know how to divide it into different mutually exclusive regions where to do so. Put in another way, can we see a molecule as a collection of smaller elements, the atoms? Is it possible to define, in a more rigorous way, based on physical principles, what is an atom inside of a molecule? The answer is given by Bader in his famous theory *Atoms in Molecules* (AIM) [15].

This theory, developed at McMaster University between the 60s and 90s, tries to provide a bridge between quantum mechanics and chemistry so that we can get some chemical insight from modern electron densities.

If we look for a partition based solely on physical principles then the answer must be contained in the wave function ( $\Psi$ ), since it is one of the postulates of quantum mechanics that all information that can be known about the system is in it. This leads us to the analysis of the electronic charge density ( $\rho$ ) and its associated gradient vector field. This vector field is a field where each point in space is assigned a vector with magnitude and direction given by the gradient of the charge density. This is usually represented by way of gradient paths that are paths obtained by calculating the gradient at a point, moving an infinitesimal distance away in the direction given by it and repeating this process until it stops at a point with gradient

zero (known as critical points). These paths are perpendicular to lines of constant density, that is to contour lines of  $\rho$ , since the gradient vector of a scalar points in the direction of greatest increase in the scalar. The vector  $\nabla\rho(\vec{r})$  is tangent to its trajectory at each point  $\vec{r}$  and trajectories cannot cross as  $\nabla\rho(\vec{r})$  defines but one direction at each point  $\vec{r}$ . An example of the gradient vector field for the molecule of  $\text{C}_2\text{H}_4$  is shown in figure 2.2.

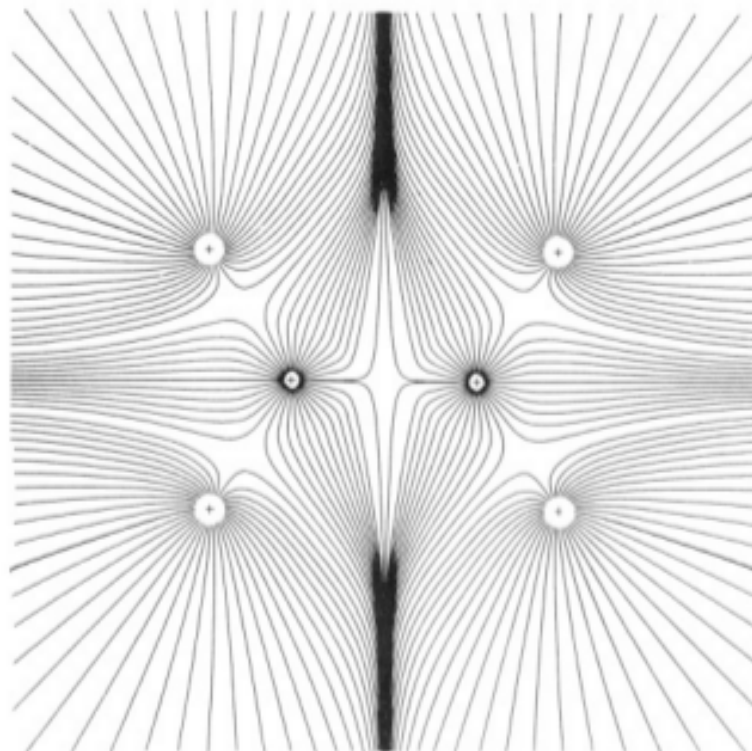


Figure 2.2: Gradient paths for the plane containing the nuclei in  $\text{C}_2\text{H}_4$ . Only paths that end at a nuclei are represented and they have been arbitrarily terminated a small distance away from the nuclei. The separation of space into different atomic basins is clearly seen. From [15].

The first characteristic we notice when looking at this field is that at the nuclear positions the charge density is maximum and all gradient paths that surround it terminate there. The nuclei behave as attractors and the region defined by all paths that terminate there is called its basin. The system is partitioned into different basins, each containing a single attractor. An atom in a molecule is, in the context of this theory, defined as an attractor and its associated basin. Looking again at figure 2.2 the division of space into six atoms can clearly be seen, with all gradient paths in the vicinity of each nucleus converging to it.

Two atoms are separated by a surface, the inter atomic surface (IAS), defined by the set of all

paths that terminate at neither of the neighboring atoms. This surface is also known as a zero flux surface since it obeys the condition:

$$\nabla\rho \cdot \vec{n} = 0 \quad (2.19)$$

That is, the IAS is not crossed by any gradient vector of  $\rho$ . The flux of the gradient of  $\rho$  is zero for all points in this surface. This condition is easy to ascertain since the gradient is tangent to the paths at each point, and therefore necessarily perpendicular to the normal to the surface that contains it. This condition is in fact valid for all points with a notable exception, the nucleus. There the density exhibits a cusp and therefore its gradient is not defined, thus equation 2.19 does not hold. What makes the IAS special is that it is the only surface formed by paths that don't pass through the nucleus, making it the only surface where the zero flux condition holds for all points.

The paths that form the IAS also end at a critical point, that belongs to the surface, called the bond critical point (BCP). This critical point differs from the one at the nuclear positions because in addition to all the paths that form the IAS there are two extra paths that start here and end at the neighboring nuclei. This happens because the density, unlike at the nuclear positions, isn't a maximum in all directions here. This is a (3,-1) critical point, meaning that the Hessian, which is a square matrix of second-order partial derivatives of a scalar field, that in this case is the charge density field, at this point has three different eigenvalues, known as the point's rank, and the sum of their signs is -1 (it has two negative eigenvalues and a positive one), known as the points signature, as opposed to the critical point at the nuclear positions which is a (3,-3) critical point. This means the density here is a maximum in the IAS and a minimum in the line formed by this two paths, which is called the atomic interaction line (AIL), since it indicates the existence of an interaction between both nuclei. The charge density is also maximum in this line with respect to neighbouring lines. If the molecule is in an energy minimum then the AIL is called a bond path (BP) and the nuclei at its end are said to be bonded. The collection of all bond paths in a molecule at its equilibrium geometry is called the molecular graph

Since in every IAS there is a BCP and the respective AIL only bonded atoms will share a surface. This means that some atoms will have somewhat weird shapes, as defined in this theory, when two physically close atoms are not bonded to each other and therefor cannot share a surface. One example of this is the shape of the boron atom in the  $\text{BH}_3$  molecule, as seen in figure 2.3

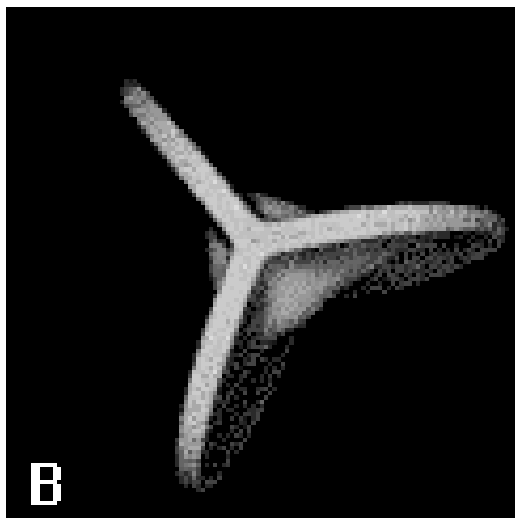


Figure 2.3: Representation of the boron atom in  $\text{BH}_3$ . The atom is bounded by the inter atomic surfaces and the  $\rho = 0.001au$  molecular envelope. From [16].

The analysis of the topology of the charge density is also able to identify other features in the molecular structure, such as rings and cages.

Rings are formed when nuclei are connected in such a way as to form a ring and are identified by a  $(3,+1)$  critical point inside it, the ring critical point (RCP). An infinite number of gradient paths originate at the RCP and terminate at either the nuclei or the BCP. The set of all these paths defines a surface called a ring surface. Two paths start at infinity and end at the RCP, forming what is called the ring line. The density is a minimum at the RCP in the ring surface and a maximum in the ring line.

Cages are formed when various rings are connected and enclose a portion of space, being identified by a  $(3,+3)$  critical point also inside of it, the cage critical point (CCP). The charge density is a minimum in three dimensions at the cage critical point, therefore no paths terminate at the CCP, they only originate there.

Another key aspect of this theory, although not as useful for the work developed here, is

the analysis of structure stability. In general the molecular graph doesn't change with the nuclear vibration. The structure of the molecule remains the same for all these slightly different geometries. Changes in molecular structure are an abrupt and discontinuous processes and can be studied by looking at how the molecular graph changes with the change in position of the atoms. These changes can occur by way of two different mechanisms: the bifurcation and the conflict mechanism.

In the bifurcation mechanism change in structure occurs when two critical points coalesce into a degenerate critical point that then disappears or the other way around, a degenerate critical point appears and then splits into to different critical points. This is illustrated in figure 2.4.

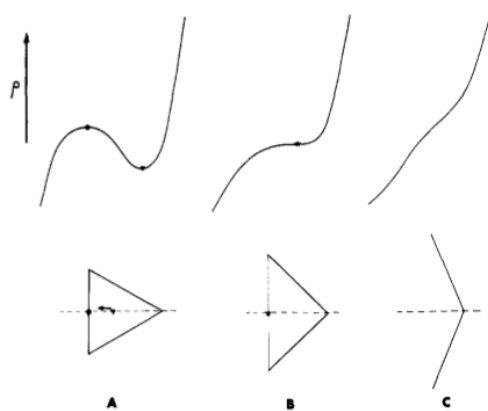


Figure 2.4: Example of the bifurcation mechanism on the opening of a ring in a three atom structure. On the top row profiles of  $\rho$  along the dashed line are represented. On the bottom row, dots represent selected critical points and lines represent bond paths between the atoms at their ends. As the RCP approaches the BCP the curvature of  $\rho$  at their positions starts to become equal. When they touch the first and second derivative at that point are zero, the critical point is degenerate. Moving further apart the critical point disappears and so does the bond, creating an open structure. From [15].

In the conflict mechanism critical points are the same but the way they are connected changes. Here a small change in the position of one of the atoms will cause the bond path to go from one attractor to another, with the mechanism's name deriving from the competition that exists between the attractors. An example of the conflict mechanism is provided in figure 2.5.

The theory of atoms in molecules gives us then, through the zero flux condition and the analysis of the gradient paths, a way, entirely based in physical principles, to partition the space into non-overlapping regions where to calculate any property of interest.



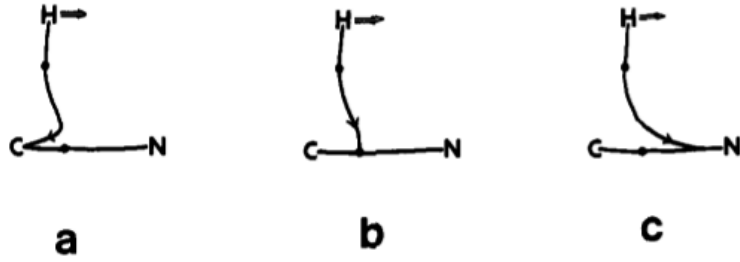


Figure 2.5: Example of the conflict mechanism in the isomerization of HCN to CNH. As the hydrogen atom moves from left to right the bond goes from the carbon atom to the nitrogen atom. Structure (b) is unstable. An infinitesimal change in the coordinates of the atoms will change the system into one of the two stable structures. From [15].

## 2.4 Local Density of States

The density of states (DOS) is a measure of the number of levels available for a system at a certain energy i.e. the number of states per unit energy. To get the DOS for a free electron gas in a cubic box of side  $L$  we start by solving the free-particle Schrödinger equation:

$$-\frac{\hbar^2}{2m} \left( \frac{\partial^2}{\partial x^2} + \frac{\partial^2}{\partial y^2} + \frac{\partial^2}{\partial z^2} \right) \psi_k(\vec{r}) = \epsilon_k \psi_k(\vec{r}) \quad (2.20)$$

The solutions of this equation that satisfy the periodic boundary conditions are [17]:

$$\psi_k(\vec{r}) = e^{i\vec{k}\cdot\vec{r}} \quad (2.21)$$

with:

$$k_x = \frac{2\pi n}{L}, \quad n = 0, \pm 1, \pm 2 \dots \quad (2.22)$$

and similarly for the  $y$  and  $z$  components. The energy for each state is :

$$\epsilon_k = \frac{\hbar^2 k^2}{2m} \quad (2.23)$$

Each state can be represented as a point inside a sphere in  $k$ -space. The total number of states is given by dividing the volume of the sphere by the volume occupied by each state:

$$N = 2 \left( \frac{L}{2\pi} \right)^3 \frac{4\pi k_F^3}{3} \quad (2.24)$$

where a factor of two was added to account for both possible spins of each solution and  $k_F$  is the Fermi radius, the value of  $k$  for the states at the surface of the sphere.

The density of states is the number of states per unit energy per volume and so, finally, to obtain it we do:

$$g(E) = \frac{1}{V} \frac{dN}{dE} = \frac{1}{2\pi^2} \left( \frac{2m}{\hbar^2} \right)^{3/2} E^{1/2} \quad (2.25)$$

where he have made use of the chain rule and equation 2.23. This density of states is represented in figure 2.6.

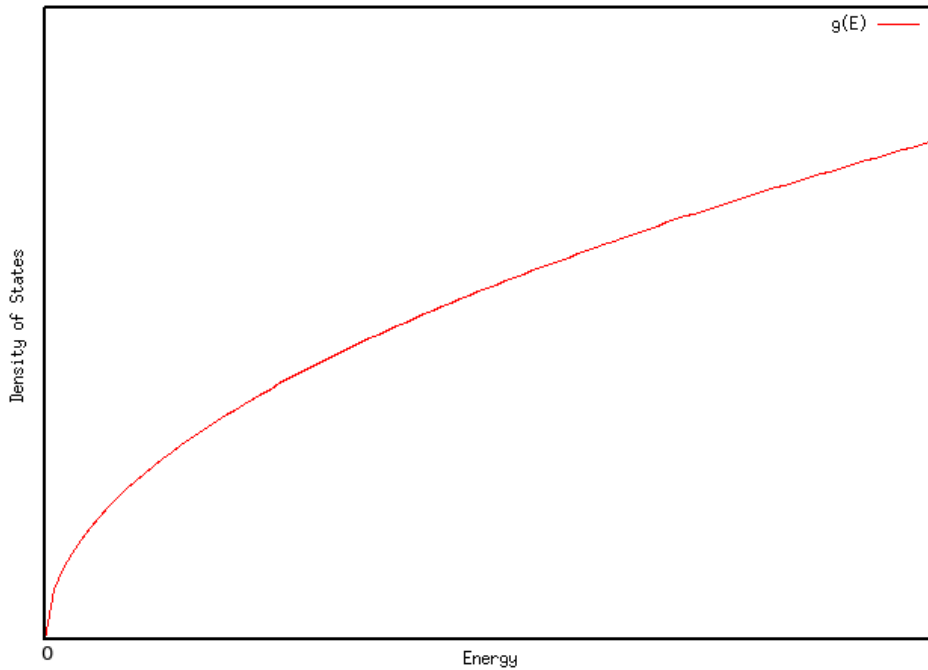


Figure 2.6: Density of states for the 3D homogeneous electron gas.

The local density of states is exactly the same thing but for a certain region of space instead of the whole system. In general for many particle systems the DOS will be a continuous function, however in our case, since we will apply this to simple molecules, the DOS will be a discrete distribution, akin to a spectral density.

# Chapter 3

## Results

### 3.1 Introduction

This chapter's objective is to expose the work done in this thesis. There are two parts to this, the division of molecules into Bader regions and the calculation of the local density of states, each assigned a sub-chapter. In each sub-chapter a brief description of the algorithm is provided as well as some examples computed in order to test the implementation.

### 3.2 Implementation of the Bader Volumes

The algorithm for the decomposition of electronic density into atomic regions, in accordance with the theory of atoms in molecules, implemented here follows that of Henkelman et al. [18].

The input for this algorithm is the value of the charge density on each point of the real-space grid. To form the different regions steepest ascent paths are calculated. This is done by starting from a given grid point and calculating the gradient of the charge density in each of

its 26 neighbors<sup>1</sup>. The charge density gradient is approximated as

$$\nabla\rho(i, j, k) \cdot \hat{r}(di, dj, dk) = \frac{\Delta\rho}{|\Delta\vec{r}|} \quad (3.1)$$

where

$$\Delta\rho = \rho(i + di, j + dj, k + dk) - \rho(i, j, k) \quad (3.2)$$

$$\Delta\vec{r} = |\vec{r}(i + di, j + dj, k + dk) - \vec{r}(i, j, k)| \quad (3.3)$$

and  $di$ ,  $dj$  and  $dk$  take the values  $\{-1,0,1\}$ . Each combination of these values for  $di$ ,  $dj$  and  $dk$  corresponds to a different neighbour and  $di = dj = dk = 0$  is skipped for it represents the original point. The steepest ascent point selected is the one that maximizes  $\nabla\rho$ . This process is then repeated in the new point and so forth until we reach a point that either already belongs to a path or where the density is maximum, that is,  $\Delta\rho$  is negative for all neighbors of this point.

One thing requiring particular attention when doing this analysis is the density in the core region. An accurate representation of the density here is needed since this is where the nuclear attractor, a maximum in the charge density in all directions, is located. A representation of the core electron density is therefore required. One needs also to be careful when using pseudopotentials seeing that in this region the pseudo-wavefunction and the true wavefunction are different. This can lead to the appearance of artificial minima which means the steepest ascent paths will no longer terminate at the nucleus and the Bader regions created will not make sense.

This algorithm is illustrated in figure 3.1. We choose point  $(i_1, j_1, k_1)$  to start the calculation and follow the steepest ascent path until we reach  $m_1$ , a maximum. At this point we need to identify all the points we passed as belonging to the same region and do so by assigning to each one the value 0, since this is the first maximum we encounter. In figure 3.1(B) we move on to point  $(i_2, j_2, k_2)$ , the next point that hasn't been assigned to a region yet. We calculate the steepest ascent path till we arrive at a point that has already been allocated to region 0

---

<sup>1</sup>Here we assume an orthogonal cubic lattice for simplicity's sake. The generalization to a non-orthogonal lattice or even a 2D or 1D one, where the number of neighbors is, respectively, 8 and 2, is straightforward.

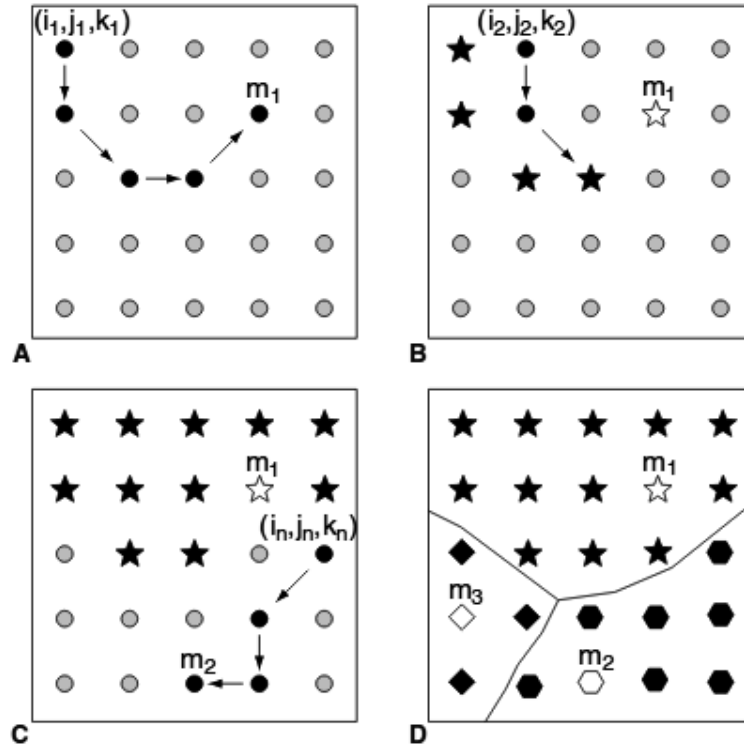


Figure 3.1: Illustration of the algorithm used to find the Bader regions. (A) the first path starts at point  $(i_1, j_1, k_1)$  and ends at  $m_1$ , a maximum in the charge density. All of these points are assigned to the same region. (B) The second path starts in the next unassigned point, point  $(i_2, j_2, k_2)$ , and terminates in a point already assigned to region 0 (represented by stars). (C) A new maximum,  $m_2$ , is found at the end of the path started at point  $(i_n, j_n, k_n)$ . All points in this new path are assigned to a new region, region 1. (D) In the end, after all points have been mapped, three distinct regions, each with its associated maximum, have been found. These are represented as stars for  $m_1$ , hexagons for  $m_2$  and diamonds for  $m_3$ . From [18].

and so we can stop and map every point of this second path onto region 0. In figure 3.1(C) a new maximum,  $m_2$ , is found, starting from point  $(i_n, j_n, k_n)$ . Since this is a new maximum each point is assigned a new value, in this case 1. Finally, when all grid points have been mapped, figure 3.1(D), the partitioning is complete and we have all of our Bader regions defined. Any property of interest, for example the total electronic charge in each region, can be calculated by summing over all points belonging to the region in case.

One big advantage of this approach is that, unlike other implementations, the critical points in  $\rho$  and the zero-flux surfaces are not explicitly calculated. This grid based analysis only requires 26 calculations and comparisons per grid point (one for each neighbour), making it scale linearly with the number of grid points.

As an example the Bader regions for a  $N_2$  molecule are shown in figure 3.2. Every point on the grid is represented and the region they belong to is shown by their color. The space is, as expected, divided into two different regions (one represented in yellow and the other in black).

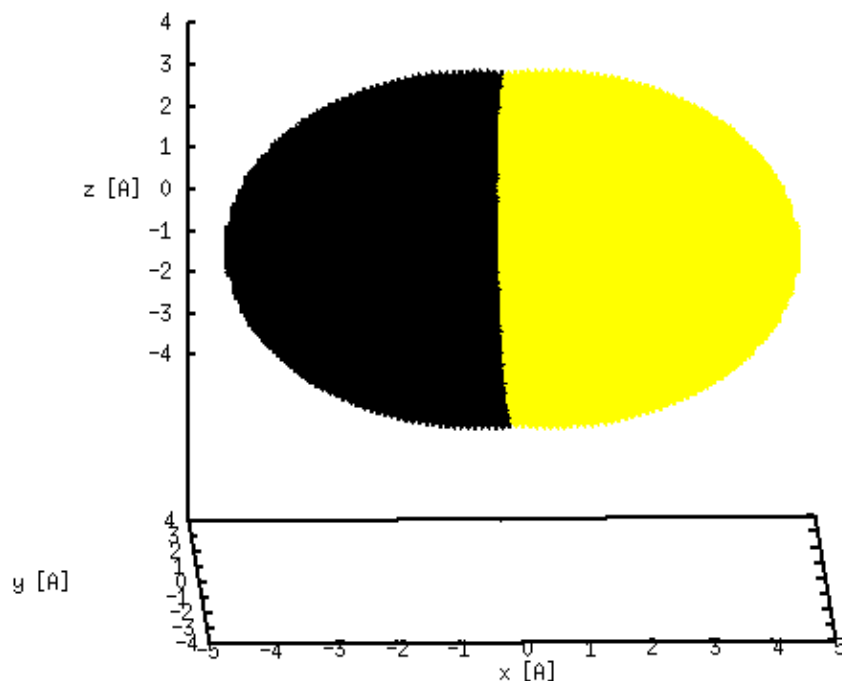
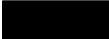



Figure 3.2: Bader regions on a  $N_2$  molecule. The two atoms are clearly visible and symmetric, as expected.

Some properties of these regions can be seen in table 3.1. The positions of the maximum points, that is, points where the charge density is maximum and where the steepest ascent paths stop, are symmetric and correspond to the nuclear positions used in the input file. The two atoms however are not totally symmetric, as their volumes and the total electronic charge inside them, although close to the expected seven electrons in each nitrogen atom, are not exactly the same. This is due to the fact that the algorithm doesn't explicitly find the critical points in the charge density field, it only follows steepest ascent paths. Because of this the inter-atomic surface, that in this case, and for symmetry reasons, falls on the  $x = 0$  plane, isn't identified, since the critical point in it isn't a maximum in all directions. Once this point is reached the gradient is computed in all neighbors, including the ones along the  $x$  axis where the density is bigger seeing that it is a minimum along the atomic interaction line at this point and so the points forming the IAS are assigned to one of the neighboring atoms. This problem can be minimized

by using a finer grid (the difference in volume and charge between the regions will be smaller) but so long as there are grid points that belong to the IAS this problem persists.

Table 3.1: Positions of the maximum, volume and population in each Bader regions on a  $N_2$  molecule.

Color	Atom	Position of MP [ $\text{\AA}$ ]	Volume [ $\text{\AA}^3$ ]	Population
	N	(-0.55, 0.00, 0.00)	158.906759	6.765612
	N	(0.55, 0.00, 0.00)	164.311950	7.234388

As a slightly more complex example the Bader regions for a methane molecule ( $CH_4$ ) were also computed and are shown in figure 3.3.

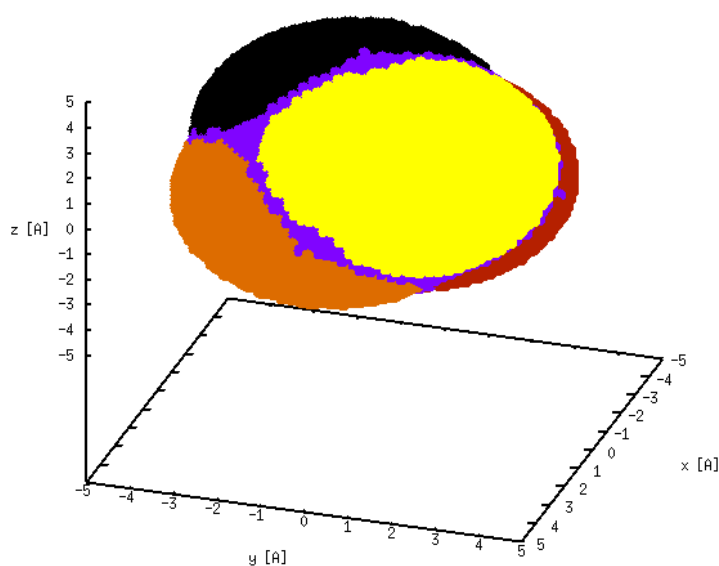







Figure 3.3: Bader regions on a methane molecule. The carbon atom is represented in purple with other colors representing each of the hydrogen atoms.

Again some properties of these regions were calculated and the results are shown in table 3.2. The positions of the maximum points are, as expected, located at the grid point nearest to the atomic positions (in the input file the carbon atom is at the origin and the hydrogen atoms are  $1.2 \text{ \AA}$  away from it, that is  $1.2/\sqrt{3} \approx 0.69 \text{ \AA}$  along each Cartesian axis and the signs are the same as in table 3.2). The hydrogen atoms are also bigger than the carbon atom. The population in each atom is close to the atomic number with the carbon atom being slightly overcharged and the hydrogen atoms undercharged. Also of note is the agreement between the hydrogen atoms, with their volume and population being the same. On a more visual note we can see the strange shape of the carbon atom. This odd shape is nonetheless expected as

the hydrogen atoms can't share a boundary, for this would imply the existence of an atomic interaction line between them and thus also of a bond.

Table 3.2: Positions of the maximum, volume and population in each Bader regions on a methane (CH<sub>4</sub>) molecule.

Color	Atom	Position of MP [Å]	Volume [Å <sup>3</sup> ]	Population
	H	(-0.72, -0.72, 0.72)	70.497216	0.906979
	C	( 0.00, 0.00, 0.00)	55.316520	6.372085
	H	(-0.72, 0.72, -0.72)	70.497216	0.906979
	H	( 0.72, -0.72, 0.72)	70.497216	0.906979
	H	( 0.72, 0.72, 0.72)	70.497216	0.906979

One final note with regards to the Bader decomposition algorithm: one must be careful with the labelling of the regions when doing a time-dependent run. The partitioning is done anew each desired iteration, as a new molecular configuration means also a new electronic density. Since regions are labelled as they are found it can happen that what used to be the third maximum to be found is now the fourth, and so what is the same region (the same nucleus, approximately the same position and a similar shape) has now a new name.

### 3.3 Calculation of the local density of states

To calculate the local density of states we start by projecting the charge density of each electronic eigenstate onto the Bader regions [19]

$$\omega_{J,i} = \int \Omega_J(\vec{r}) \rho_i(\vec{r}) d\vec{r} \quad (3.4)$$

where  $\Omega_J(\vec{r})$  is 1 inside the Bader region with index  $J$  and 0 outside of it. The local DOS is then the projection of the total DOS in the Bader region, with each state weighted by  $\omega_{J,i}$

$$DOS_J(\epsilon) = \sum_i \delta(\epsilon_i - \epsilon) \omega_{J,i} \quad (3.5)$$

where  $\epsilon_i$  is the energy of eigenstate  $i$ . To work around numerical imprecisions the  $\delta$  in (3.5) is not a true  $\delta$ . Alternatively, states whose energies differ by less than 0.01 meV are considered



to have the same energy.

Since the Bader regions are mutually exclusive and fill all space the sum of all projection weights for each state must be 1:

$$\sum_J \omega_{J,i} = 1 \quad (3.6)$$

otherwise the sum for all volumes of the local DOS would not be equal to the total DOS.

The code thus outputs a value for the local density of states for each Bader region and each energy level.

As an example, the local density of states for the betaine ( $C_5H_{11}NO_2$ ) molecule was calculated.

The structure of this molecule is represented in figure 3.4.

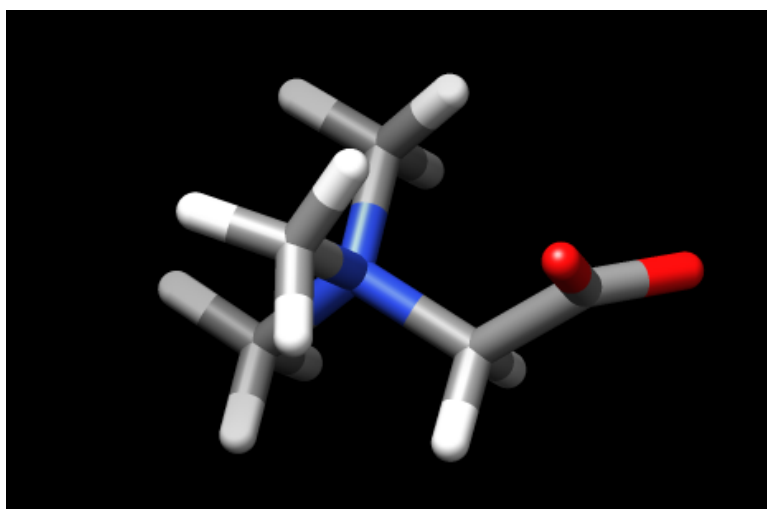


Figure 3.4: 3D configuration of the betaine molecule. The nitrogen atom is represented in blue, the carbon atoms in gray, the oxygen atoms in red and the hydrogen atoms in white.

One inconvenient aspect of using Bader decomposition is that since each region corresponds to an atom, in bigger molecules the number of regions becomes too big to be useful. To alleviate this problem all atoms were assigned to two bigger regions, as illustrated in figure 3.5. Region 0 consists of the two oxygen atoms as well as a carbon and two hydrogen ones and region 1 is made up of the remaining atoms.

The density of states for these two regions is represented in figure 3.6, where the DOS is represented for one region in each panel. Region 0 is represented in the upper panel and region

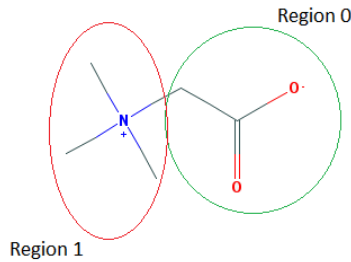


Figure 3.5: Scheme of the partition of the betaine molecule into two larger regions. Carbon atoms are represented by the vertexes of line segments and hydrogen atoms attached to carbon atoms are implied.

1 in the lower panel and the height of each impulse has the value of the density of states at that energy level for that region. The majority of energy levels are between -30 and 0 eV and so subsequent discussions will focus on this region. As for the lower energy levels, one notices the density of states for each of them is approximately 0 in one region and 2 in the other, indicating that these states are highly localized in one of the regions. The value of 2 for the density of states is due to the spin as there are two states with the same energy, one for each spin case.

In order to see the evolution of the density of states in each bigger region in time a time-dependent run was made, using the Octopus code. The molecule was excited with a laser, depicted in figure 3.7.

This laser is applied along the  $x$  direction and it is enveloped by a co-sinusoidal function as given by equation 3.7.

$$f(t) = F_0 \cos\left(\frac{\pi t - 2\tau_0 - t_0}{2\tau_0}\right) \quad (3.7)$$

This function goes to zero, meaning the laser is shut off, when  $|t - t_0| > \tau_0$ . The values used for this enveloping function are presented in table 3.3.

Table 3.3: Parameters used for the laser envelope function.  $f$  is the value of the frequency of the laser.

$F_0$ [eV/Å]	$\tau_0$ [ $\hbar$ /eV]	$t_0$ [ $\hbar$ /eV]
3	$2/f$	$\tau_0$

The value of  $\tau_0$  was set as a multiple of the period of the laser so that the number of oscillations was whole. In this case, and because  $t_0 = \tau_0$ , the laser does four periods. The laser has an

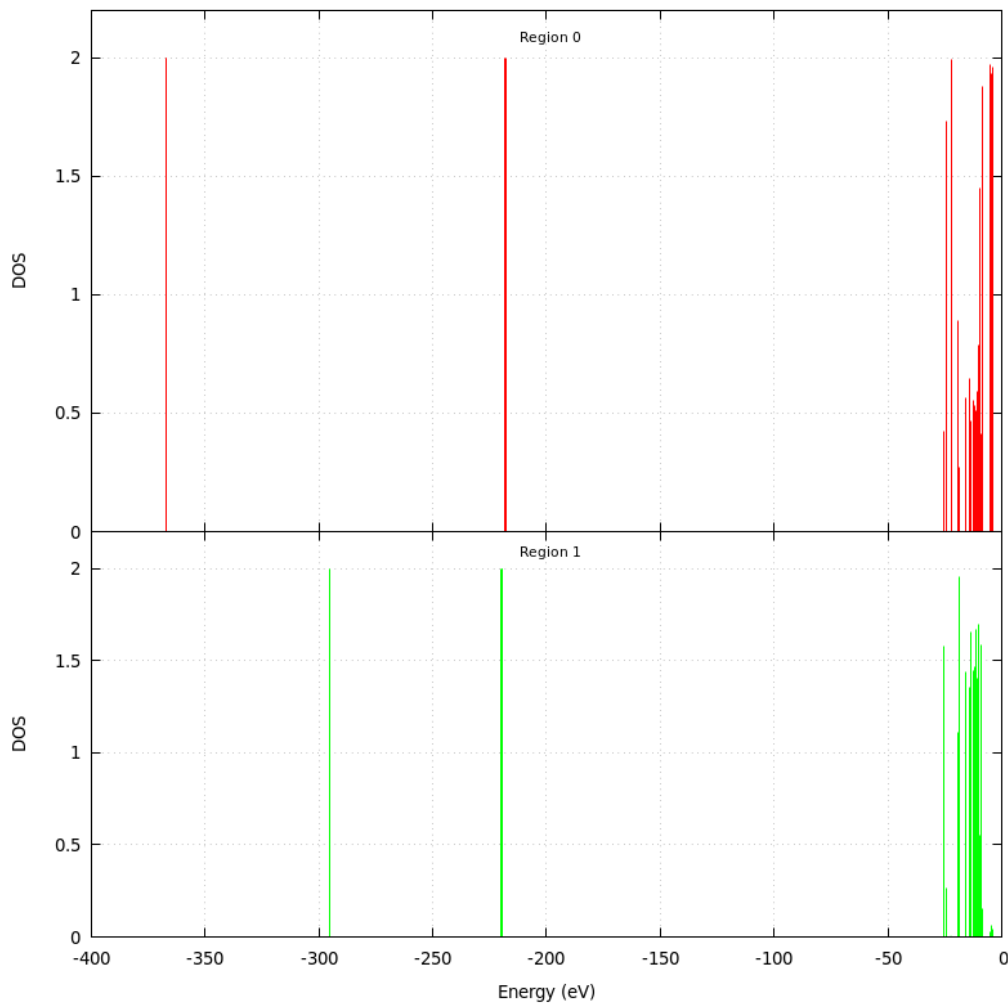


Figure 3.6: Local density of states for the betaine molecule. Each panel represents the density of states in one region. In the upper panel is the DOS for region 0 ( in red) and in the lower panel is the DOS for region 1 (in green).

energy of 13.87781 eV, corresponding to the energy of a big peak in the absorption spectrum of the betaine molecule, as observed in figure 3.8. This spectrum was obtained through a Casida run on the Octopus code.

The density of states was then calculated each 250 iterations (each corresponding to  $0.0001 \hbar/\text{eV}$ ), and is represented, for selected iterations, in figures 3.9, 3.10 and 3.11. For the remaining iterations see appendix B.

These iteration were selected because they are near a maximum of the laser (iteration 1000),

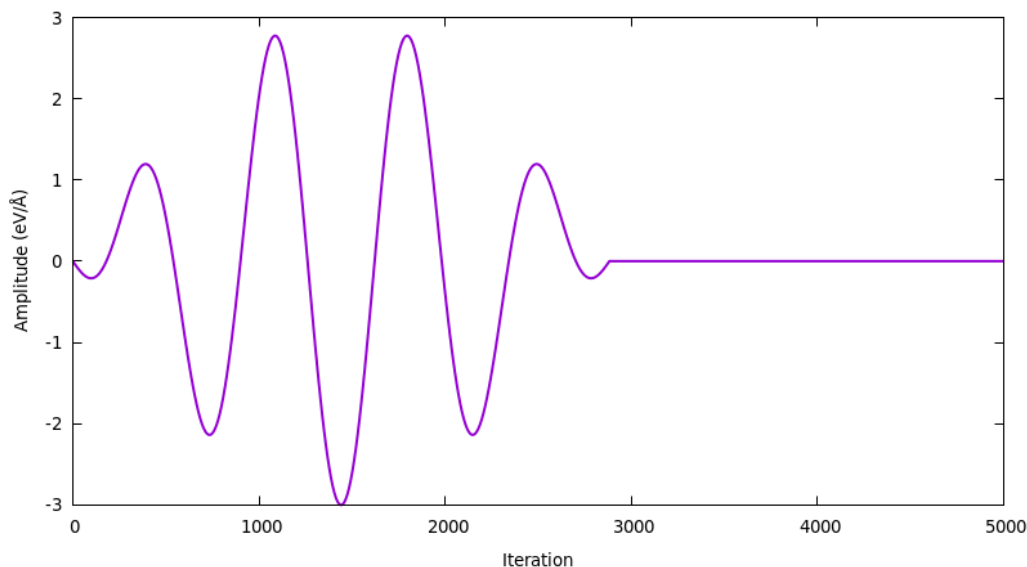


Figure 3.7: Laser field used in the time-dependent run to excite the betaine molecule. Each iteration corresponds to a time interval of  $0.0001 \hbar/eV$ .

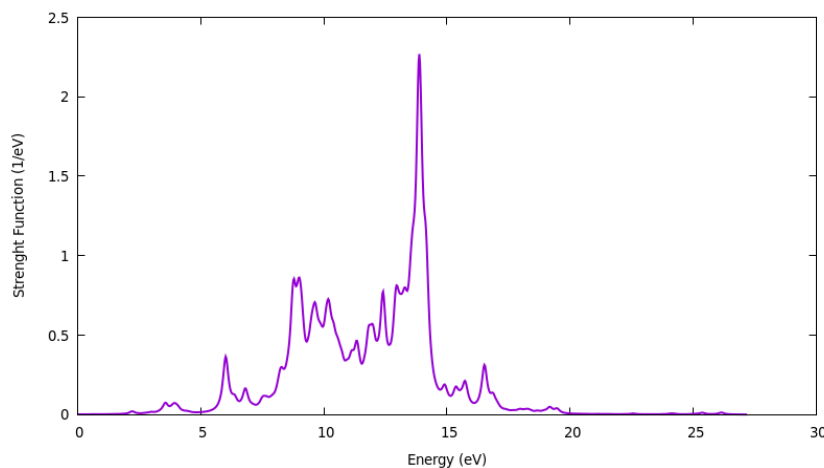


Figure 3.8: Absorption spectrum for the betaine molecule.

near a minimum of the laser (iteration 1500) and slightly after the laser being turned off (iteration 3000). We see the energy levels shift under influence of the laser. In iteration 1000 most energy level are under what they were initially and by iteration 1500 they are mostly over it. This is especially clear in the three highest energy levels as they cross the  $-5$  eV mark between iterations. After the laser shuts off the values for the density of states remain approximately constant and the energy levels are close to what they were in the beginning. Changes in the value of the DOS for each energy level, where it would decrease in one region and increase in the other thus indicating some movement of charge from one region to the other, are small and hard to see. To make this more perceptible the sum of all population in each region through

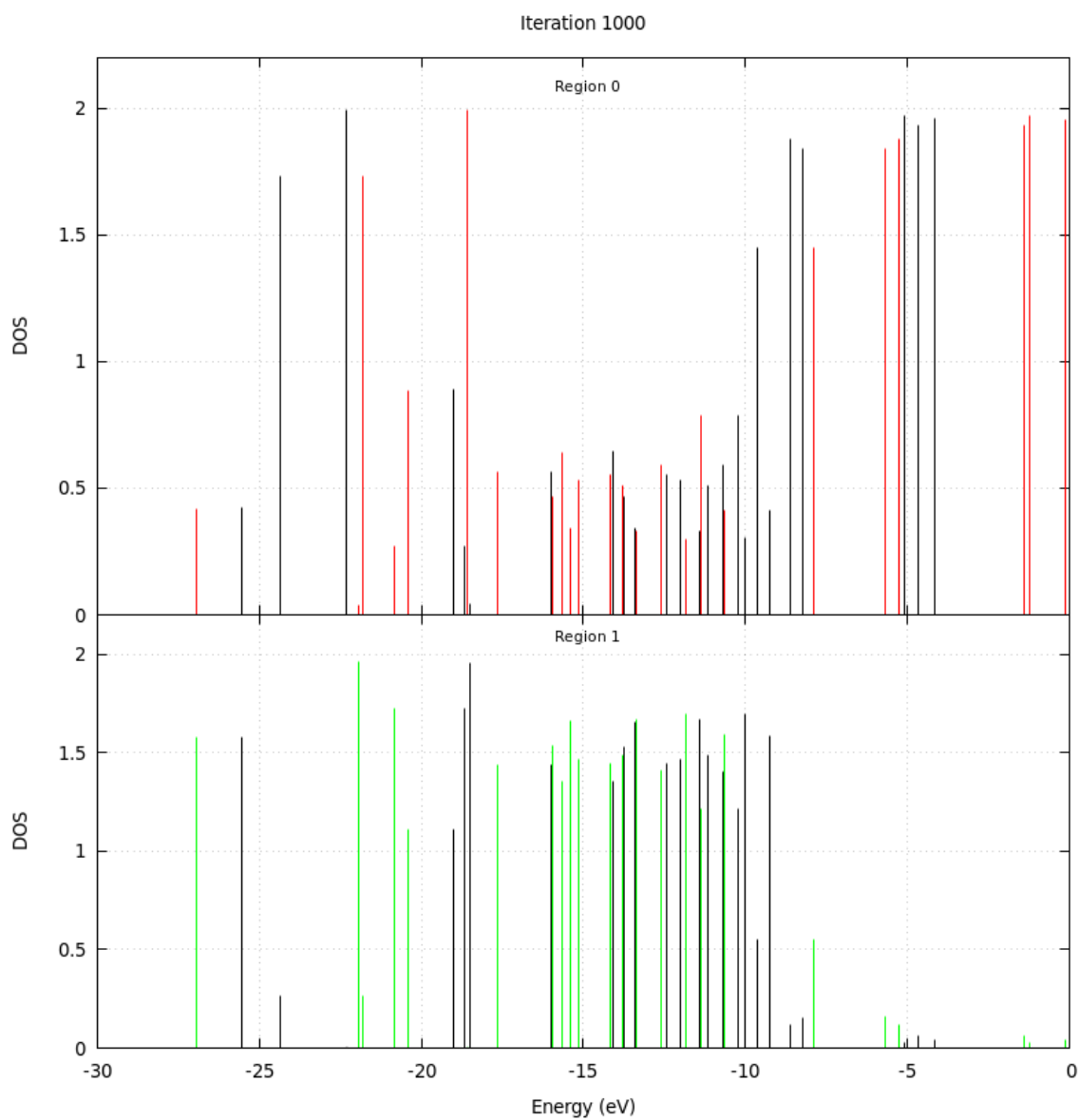


Figure 3.9: Local density of states in the betaine molecule for iteration 1000. Each impulse represents the value of the density of states for an energy level in one region. Values for region 0 are represented in the upper panel in red and for region 1 in the lower panel in green. The black impulses represent the density of states in iteration 0 and serve as a comparison point.

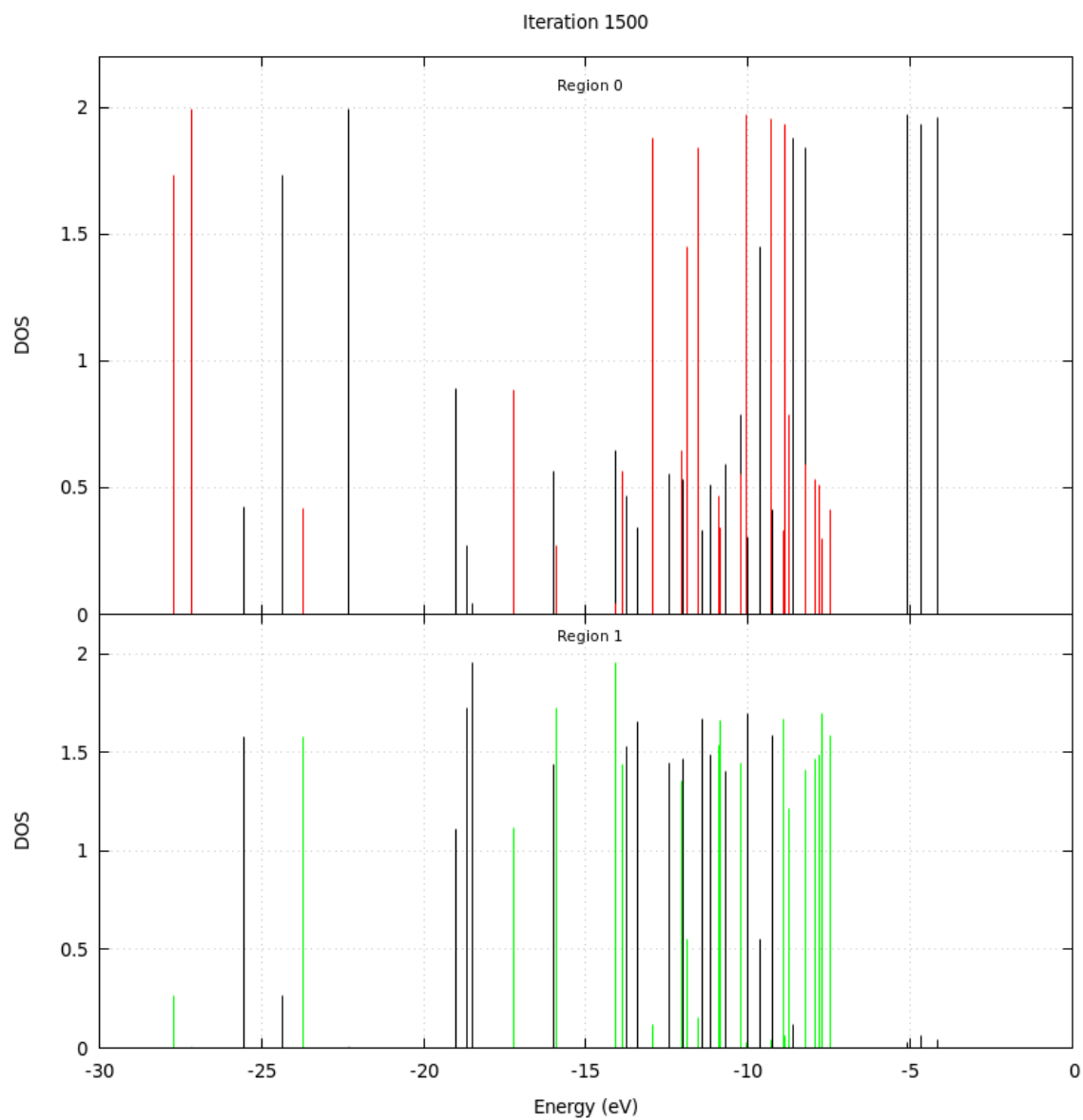


Figure 3.10: Local density of states in the betaine molecule for iteration 1500. For a detailed explanation of what is represented see figure 3.9.

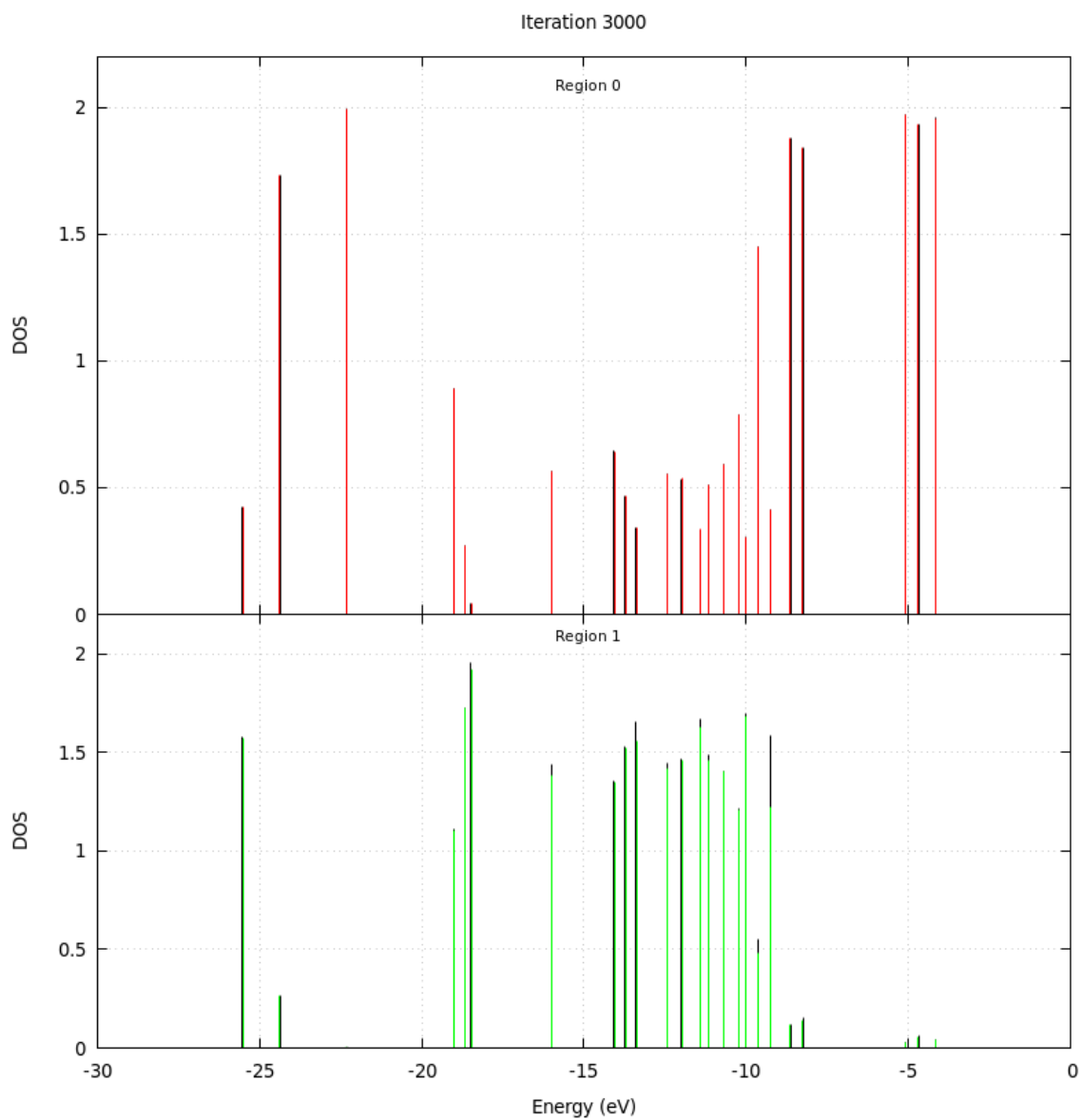


Figure 3.11: Local density of states in the betaine molecule for iteration 3000. For a detailed explanation of what is represented see figure 3.9.

time is represented in figure 3.12.

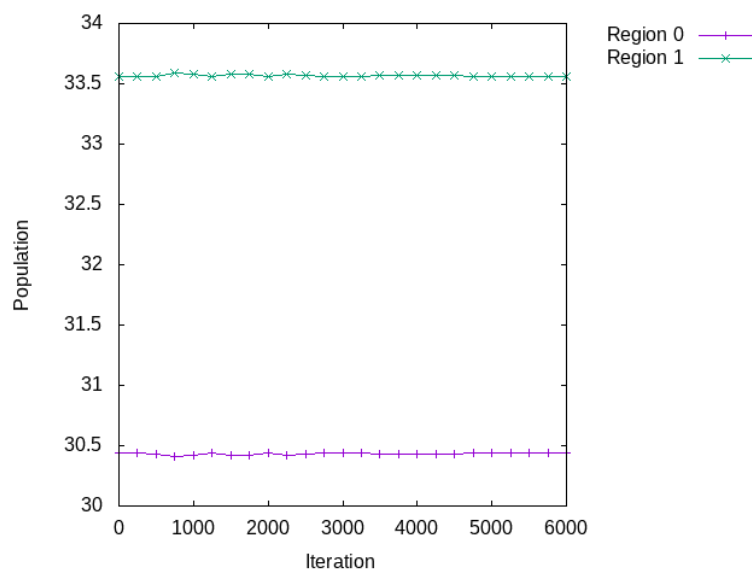


Figure 3.12: Change in population in each of the betaine regions in time. Each point represents the total population in a region for one iteration. To make changes clearer each successive point is connected with a line.

Exchange of charge between the region is apparent, although small (in the order of the decimals), principally when the molecule is under the effects of the laser.

As another example the local density of states was again calculated, this time for the for the nitroaniline ( $C_6H_6N_2O_2$ ) molecule. Figure 3.13 illustrates the structure of this molecule.

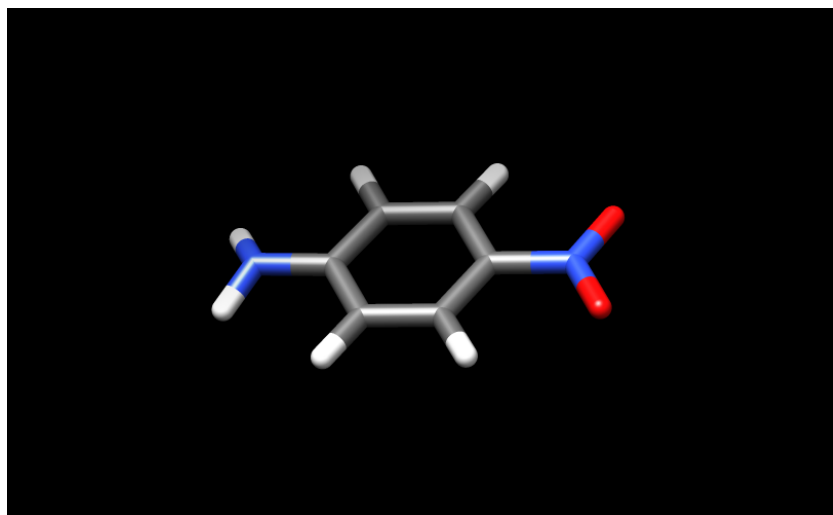


Figure 3.13: 3D configuration of the nitroaniline molecule. Again the nitrogen atoms are represented in blue, the carbon atoms in gray, the oxygen atoms in red and the hydrogen atoms in white.

Once again, in order to make the data more clear, the atomic regions were assigned to bigger



regions, as illustrated in figure 3.14. Region 0 consists of two hydrogen atoms as well as a nitrogen one, region 1 consists of the two oxygen atoms plus a nitrogen one and region 2 is made up of the remaining atoms, those that form the central ring and the respective hydrogen atoms.

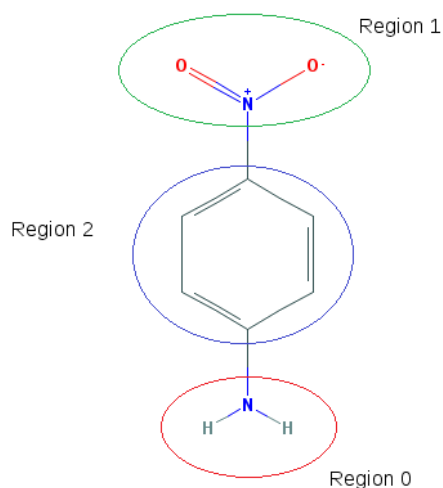


Figure 3.14: Scheme of the partition of the nitroaniline molecule into three larger regions. Again carbon atoms are represented by the vertexes of line segments and hydrogen atoms attached to carbon atoms are implied.

The density of states for these regions is represented in figure 3.15, where again each panel represents one of the regions. As in the betaine case the majority of energy levels are between -30 and 0 eV and we will again focus on this region. Once again for the lower energy levels the density of states is approximately 2 in one region and 0 in the others, again indicating that these states are highly localized in one of the regions.

A time-dependent run was also done for this molecule, using the Octopus code, to again see the evolution of the density of states in each bigger region.

The molecule was excited with a laser, depicted in figure 3.16.

This laser was applied in the same direction and has the same envelope function as the previous one. The parameters for the laser are collected in table 3.4.

This time the laser only does one period. The laser has an energy of 3.88490141 eV, correspond-

Table 3.4: Parameters used for the laser envelope function in the nitroaniline case.  $f$  is again the value of the frequency of the laser.

$$\frac{F_0 [\text{eV}/\text{\AA}]}{4} \quad \frac{\tau_0 [\hbar/\text{eV}]}{1/4f} \quad \frac{t_0 [\hbar/\text{eV}]}{\tau_0}$$

ing to the energy of the first big peak in the absorption spectrum of the nitroaniline molecule, again obtained through a Casida run on the Octopus code and depicted in figure 3.17.

The density of states was then calculated each 100 iterations (each corresponding to 0.0001  $\hbar/\text{eV}$ ), and is represented, for selected iterations, in figures 3.18, 3.19 and 3.20.

Again these iterations were selected because they are near the maximum of the laser (iteration 400), near the minimum of the laser (iteration 800) and after the laser being turned off (iteration 1400). As in the betaine case the energy levels shift up and down under the influence of the laser. Here the energy levels are shifted down when the laser is at the minimum in iteration 400 and shifted up when the laser is near a maximum in iteration 800. In iteration 1400, after the laser is turned off the energy levels are again close to the initial ones. Like in the betaine case the sum of all population in each region through time was calculated and is represented in figure 3.21.

There is a small change in charge, also in the order of 0.1 electrons, although here it is more difficult to see, given the difference in charge between regions.

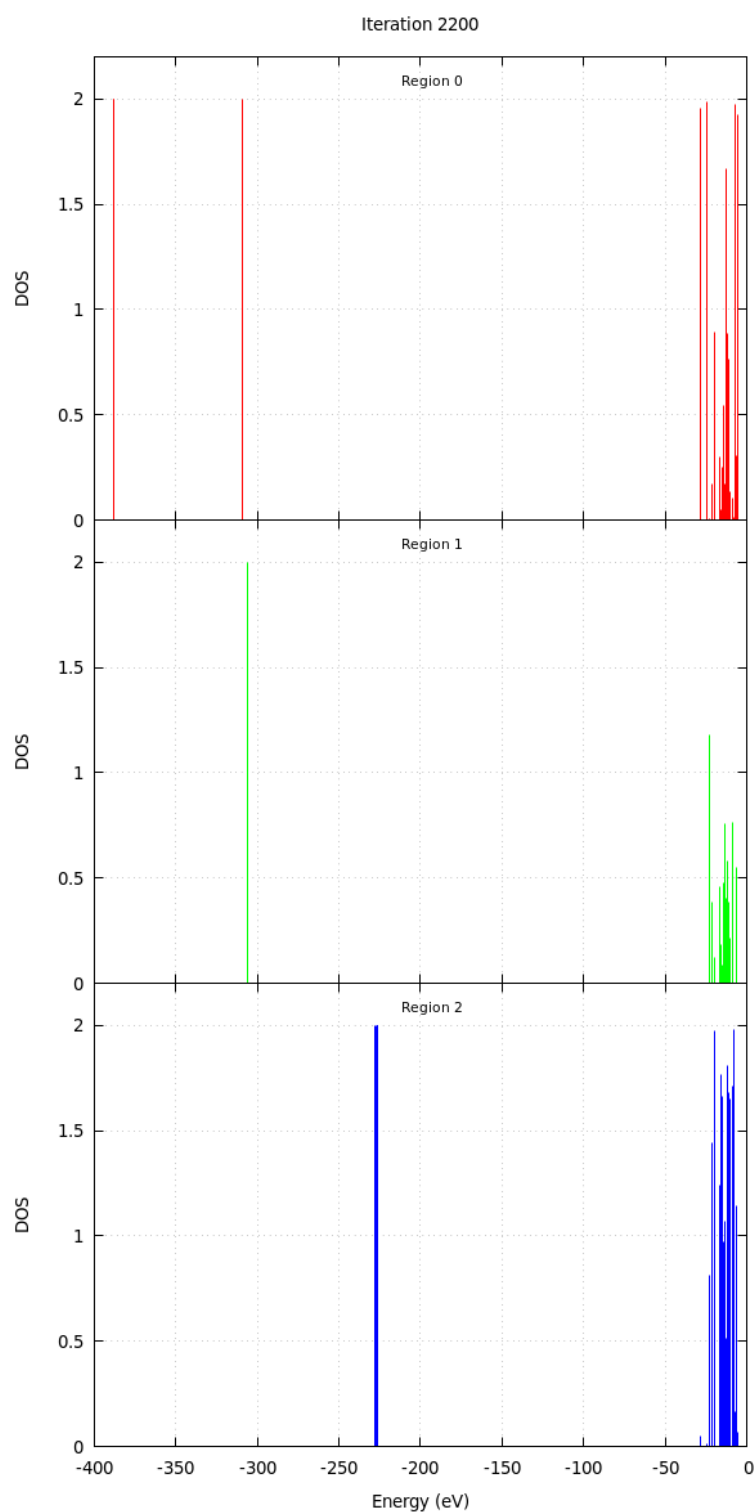


Figure 3.15: Local density of states for the nitroaniline molecule. Each panel represents the density of states in one region. In the upper panel is the DOS for region 0 (in red), in the middle panel is the DOS for region 1 (in green) and in the lower panel is the DOS for region 2 (in blue).

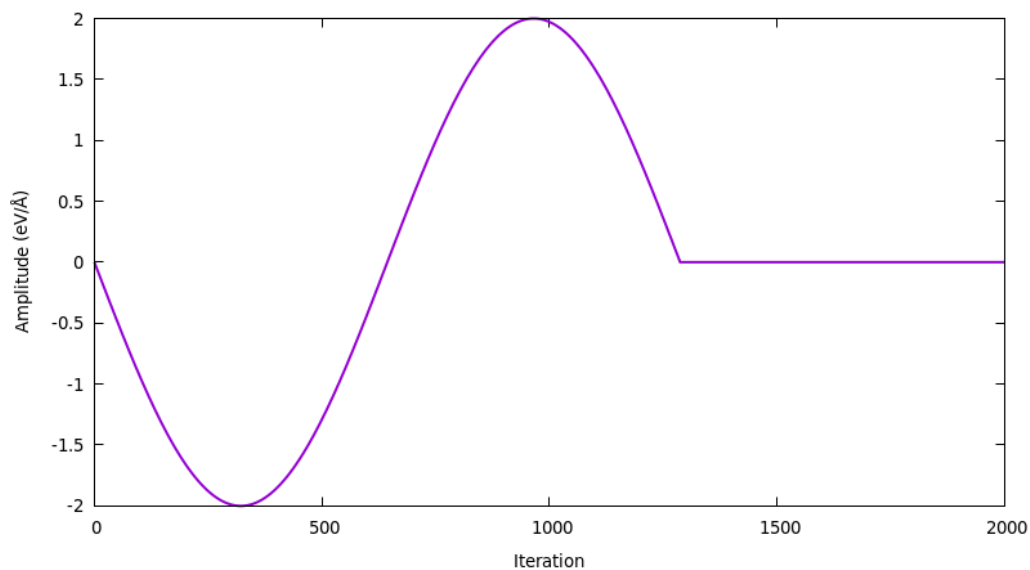


Figure 3.16: Laser field used in the time-dependent run to excite the nitroaniline molecule. Each iteration corresponds once again to a time interval of  $0.0001 \hbar/\text{eV}$ .

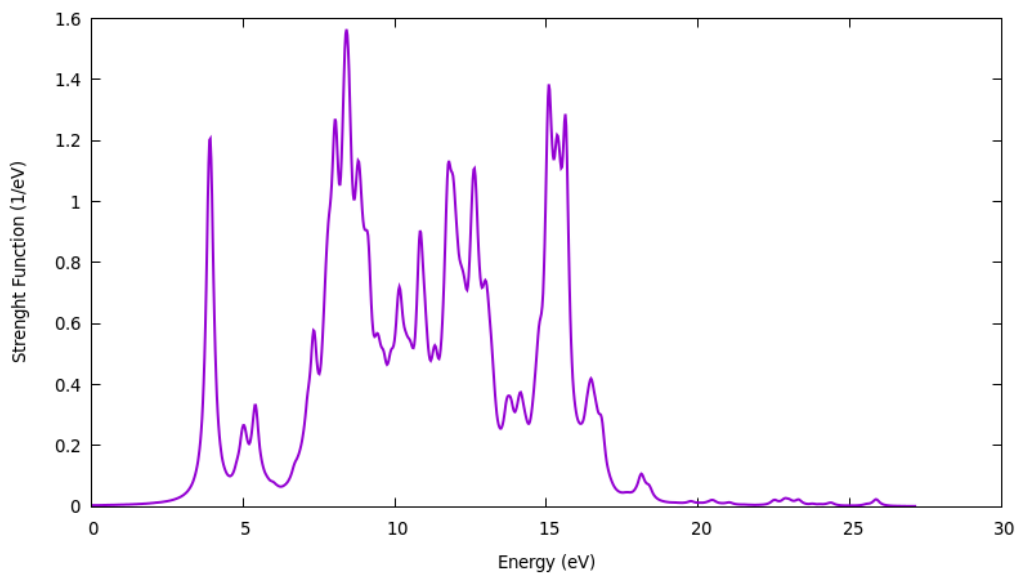


Figure 3.17: Absorption spectrum for the nitroaniline molecule.

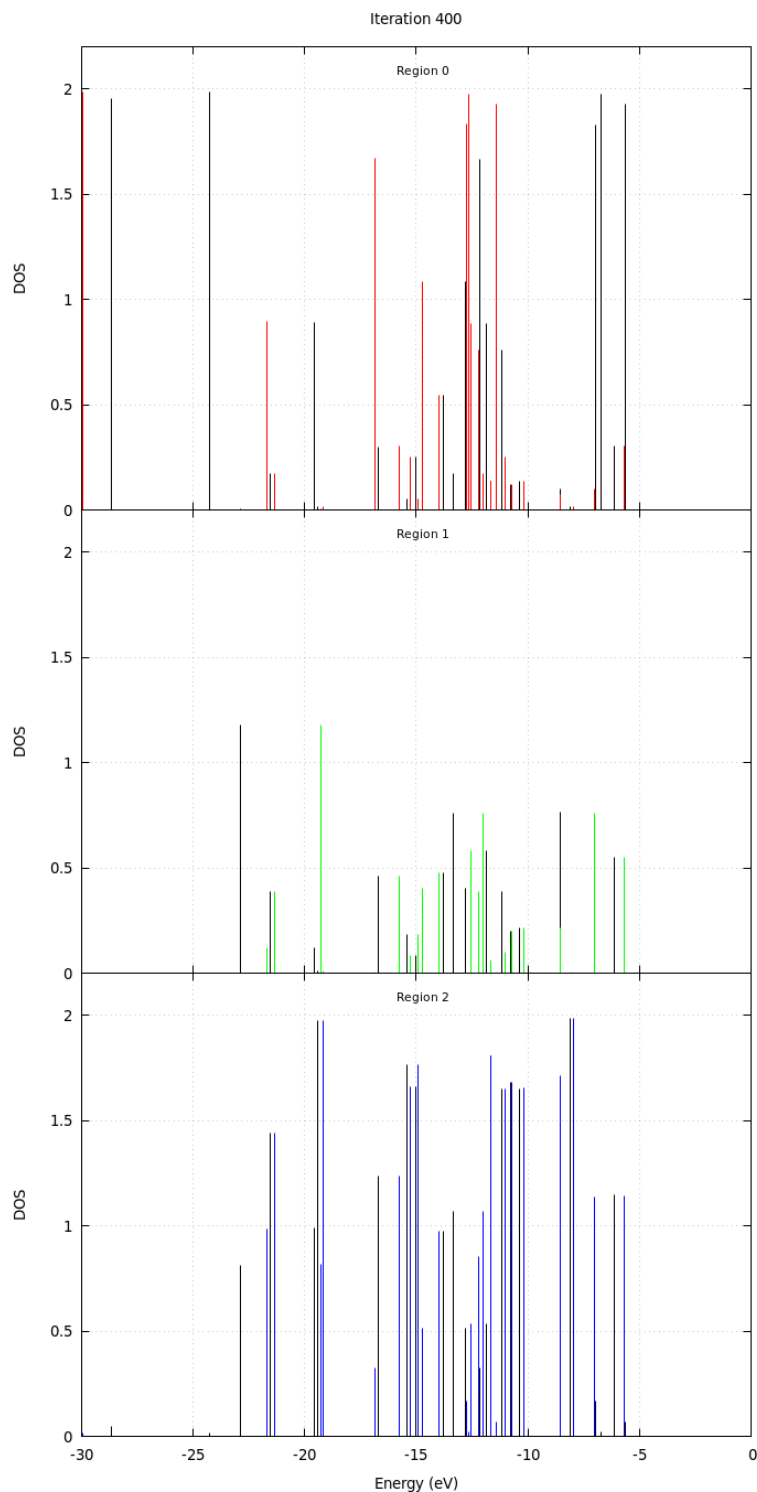


Figure 3.18: Local density of states in the nitroaniline molecule in iteration 400. Each impulse again represents the value of the density of states for an energy level in one region. Values for region 0 are represented in the upper panel in red, for region 1 in the middle panel in green and for region 2 in blue in the lower panel. The black impulses represent, as in the betaine case, the density of states in iteration 0 and again serve as a comparison point.

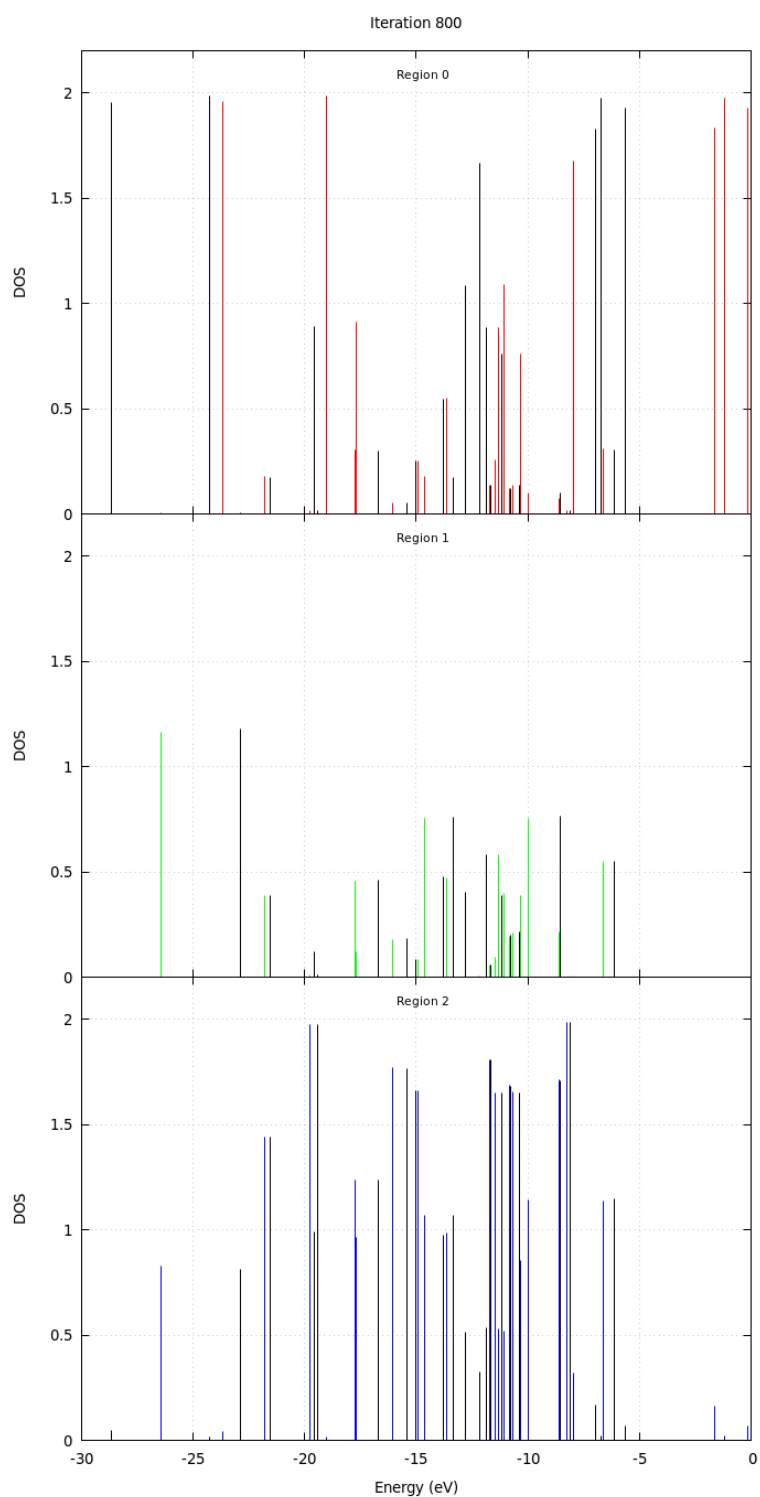


Figure 3.19: Local density of states in the nitroaniline molecule for iteration 800. For a detailed explanation of what is represented see figure 3.18.

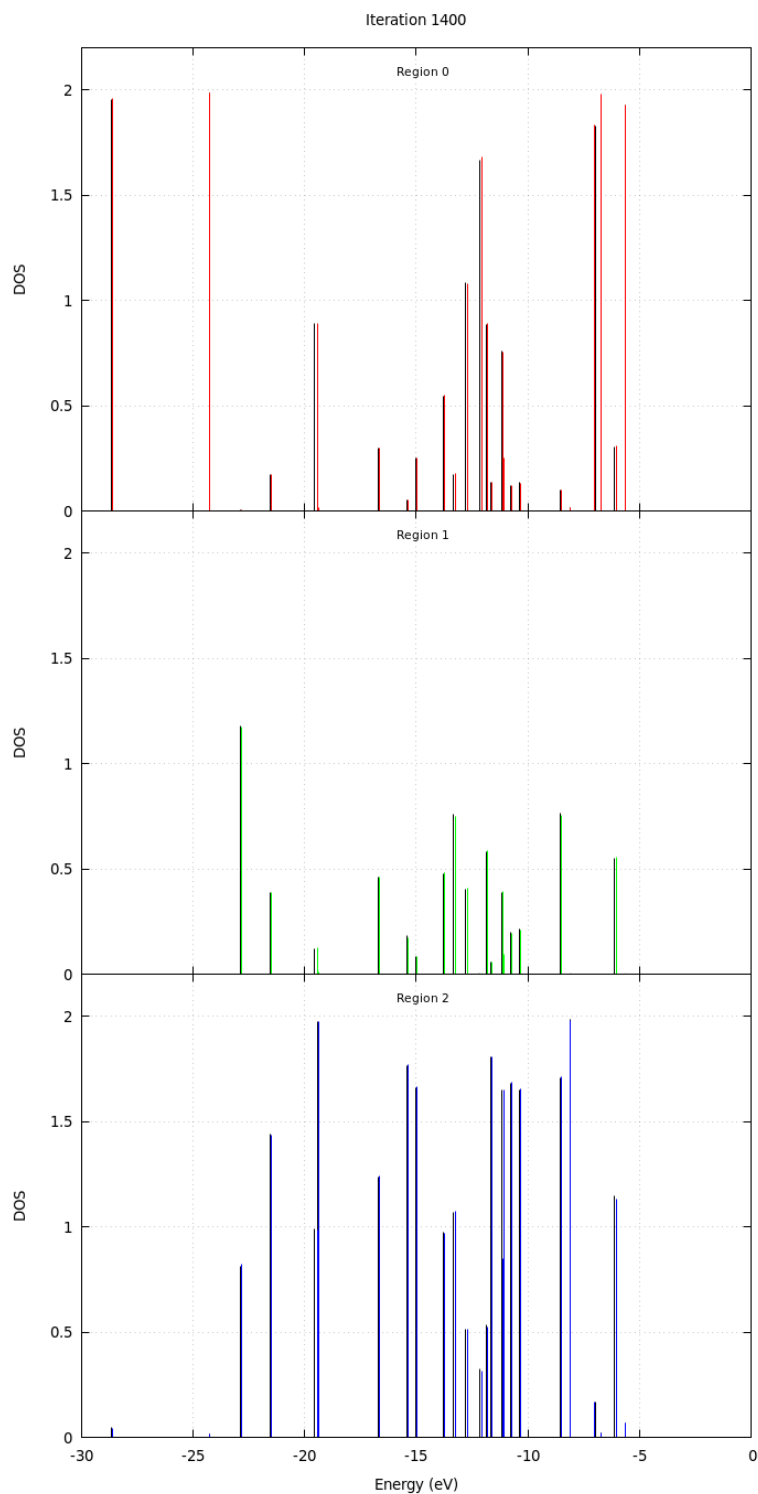


Figure 3.20: Local density of states in the nitroaniline molecule for iteration 1400. For a detailed explanation of what is represented see figure 3.18.

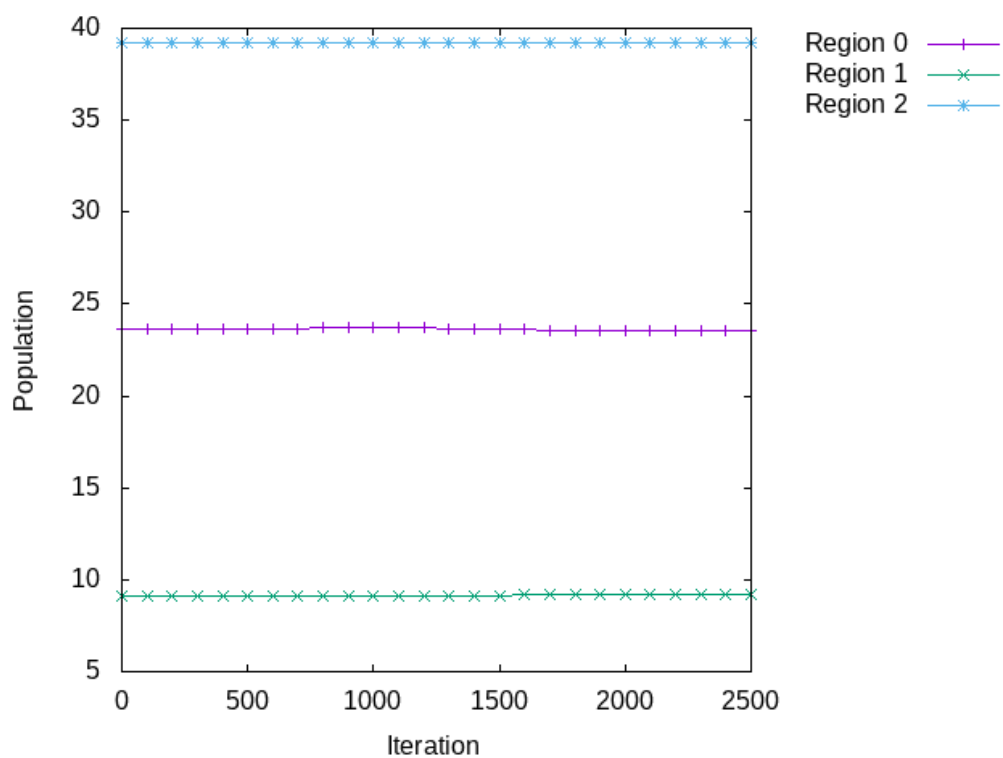


Figure 3.21: Change in population in each of the nitroaniline regions in time. As in the betaine case each point represents the total population in a region for one iteration. To make changes clearer each successive point is again connected with a line.



# Chapter 4

## Conclusion and Future work

### 4.1 Conclusion

The time-dependent local density of states is another tool to be used in trying to get a better understanding of photosynthesis. In the present work the calculation of this property was implemented in the Octopus code and some test runs were made.

The calculation for the betaine molecule here exemplified shows how correlations between energy levels in different spatial regions of a molecule can be seen with the help of the time-dependent local density of states.

The work here developed hopefully paves the way for the study of the local DOS to be applied to a myriad of structures of interest.

### 4.2 Future Work

As for future work one useful addition would be to parallelize the code, since right now it only works in serial. This would make possible calculations for bigger molecules, where the number of calculations required make it impossible to do so presently.

Another convenient extension would be to implement a way to add the core density to the valence density so that calculations using pseudopotentials can be made instead of only all electron calculations working.

# Bibliography

- [1] T. Förster. Zwischenmolekulare energiewanderung und fluoreszenz. *Ann. Phys.*, 437:55–75, 1948.
- [2] S. P. Long. We need winners in the race to increase photosynthesis in rice, whether from conventional breeding, biotechnology or both. *Plant, Cell Environ*, 37:19–21, 2014.
- [3] K. Amarnath G. R. Fleming, G. S. Schlau-Cohen and J. Zaks. Design principles of photosynthetic light-harvesting. *Faraday Discuss.*, 155:27–41, 2012.
- [4] B. F. Milne X. Andrade M. A. L. Marques F. Nogueira M. J. T. Oliveira J. J. P. Stewart J. Jornet-Somoza, J. Alberdi-Rodriguez and A. Rubio. Insights into colour-tuning of chlorophyll optical response in green plants. *Phys. Chem. Chem. Phys.*, 17:26599–26606, 2015.
- [5] U. De Giovannini A. H. Larsen M. J. T. Oliveira J. Alberdi-Rodriguez A. Varas I. Theophilou N. Helbig M. J. Verstraete L. Stella F. Nogueira A. Aspuru-Guzik A. Castro M. A. L. Marques X. Andrade, D. Strubbe and A. Rubio. Real-space grids and the octopus code as tools for the development of new simulation approaches for electronic systems. *Phys. Chem. Chem. Phys.*, 17:31371–31396, 2015.
- [6] P. Hohenberg and W. Kohn. Inhomogeneous electron gas. *Physical Review B*, 136:B864–B871, 1964.
- [7] W. Kohn and L.J. Sham. Self-consistent equations including exchange and correlation effects. *Physical Review*, 140:A1133–A1138, 1965.

- [8] D. M. Ceperley and B. J. Alder. Ground state of the electron gas by a stochastic method. *Phys. Rev. Lett.*, 45:566–569, 1980.
- [9] F. Nogueira C. Fiolhais and M.A.L. Marques. *A primer in density functional theory*. Springer, New York, 2003.
- [10] John P. Perdew, J. A. Chevary, S. H. Vosko, Koblar A. Jackson, Mark R. Pederson, D. J. Singh, and Carlos Fiolhais. Atoms, molecules, solids, and surfaces: Applications of the generalized gradient approximation for exchange and correlation. *Phys. Rev. B*, 46:6671–6687, 1992.
- [11] Swapan K. Ghosh and Robert G. Parr. Phase-space approach to the exchange-energy functional of density-functional theory. *Phys. Rev. A*, 34:785–791, Aug 1986.
- [12] John P. Perdew and Karla Schmidt. Jacob’s ladder of density functional approximations for the exchange-correlation energy. *AIP Conference Proceedings*, 577(1):1–20, 2001.
- [13] E. Runge and E. K. U. Gross. Density-functional theory for time-dependent systems. *Phys. Rev. Lett.*, 52:997–1000, 1984.
- [14] F. Nogueira E. Gross M.A.L. Marques, N. Maitra and A. Rubio. *Fundamentals of time-dependent density functional theory*. Springer-Verlag, New York, 2012.
- [15] R. Bader. Atoms in molecules. *Acc. Chem. Res.*, 18:9–15, 1985.
- [16] P.L.A. Popelier R.F.K. Bader and T.A. Keith. Theoretical definition of a functional group and the molecular orbital paradigm. *Angewandte Chemie International Edition in English*, 33(6):620–631, 1994.
- [17] C. Kittel. *Introduction to Solid State Physics*. Wiley, 7 edition, 1996.
- [18] A. Arnaldsson G. Henkelman and H. Jónsson. A fast and robust algorithm for bader decomposition of charge density. *Comput. Mater. Sci.*, 36:354–360, 2006.
- [19] G. Henkelman H Jónsson S. Gudmundsdóttir, W. Tang and E. Skúlason. Local density of states analysis using bader decomposition for  $n_2$  and  $co_2$  adsorbed on pt(110)-(1×2) electrodes. *J. Chem. Phys.*, 137:164705, 2012.

# Appendix A

## Demonstration of the first Hohenberg-Kohn theorem

Consider two external potentials,  $v_1^{ext}(\vec{r})$  and  $v_2^{ext}(\vec{r})$ , differing by more than a constant and both resulting in the same ground state density,  $\rho(\vec{r})$ . They then give rise to two different Hamiltonians,  $H_1$  and  $H_2$ , which in turn result in two distinct wavefunctions,  $\Psi_1(\vec{r})$  and  $\Psi_2(\vec{r})$ . No wavefunction can give a smaller energy for  $H_1$  than  $\Psi_1(\vec{r})$  and so we have:

$$E_1 = \langle \Psi_1 | H_1 | \Psi_1 \rangle < \langle \Psi_2 | H_1 | \Psi_2 \rangle \quad (\text{A.1})$$

Now, since both Hamiltonians have the same ground state and they differ only by the external potential we can write:

$$\langle \Psi_2 | H_1 | \Psi_2 \rangle = \langle \Psi_2 | H_2 | \Psi_2 \rangle + \int d\vec{r} [v_1^{ext}(\vec{r}) - v_2^{ext}(\vec{r})] \rho(\vec{r}) \quad (\text{A.2})$$

Substituting into (A.1):

$$E_1 < E_2 + \int d\vec{r} [v_1^{ext}(\vec{r}) - v_2^{ext}(\vec{r})] \rho(\vec{r}) \quad (\text{A.3})$$

Doing the same thing but interchanging the labels we get:

$$\langle \Psi_1 | H_2 | \Psi_1 \rangle = \langle \Psi_1 | H_1 | \Psi_1 \rangle + \int d\vec{r} [v_2^{ext}(\vec{r}) - v_1^{ext}(\vec{r})] \rho(\vec{r}) \quad (\text{A.4})$$

$$E_2 < E_1 + \int d\vec{r} [v_2^{ext}(\vec{r}) - v_1^{ext}(\vec{r})] \rho(\vec{r}) \quad (\text{A.5})$$

Summing (A.3) and (A.5) we obtain:

$$E_1 + E_2 < E_2 + E_1 \quad (\text{A.6})$$

which is obviously false and so we have demonstrated the first Hohenberg-Kohn theorem by *reductio ad absurdum*.

## Appendix B

# Local density of states in the betaine molecule for the remaining iterations.

Here the local density of states in the betaine molecule for iterations not represented in the main text are presented.

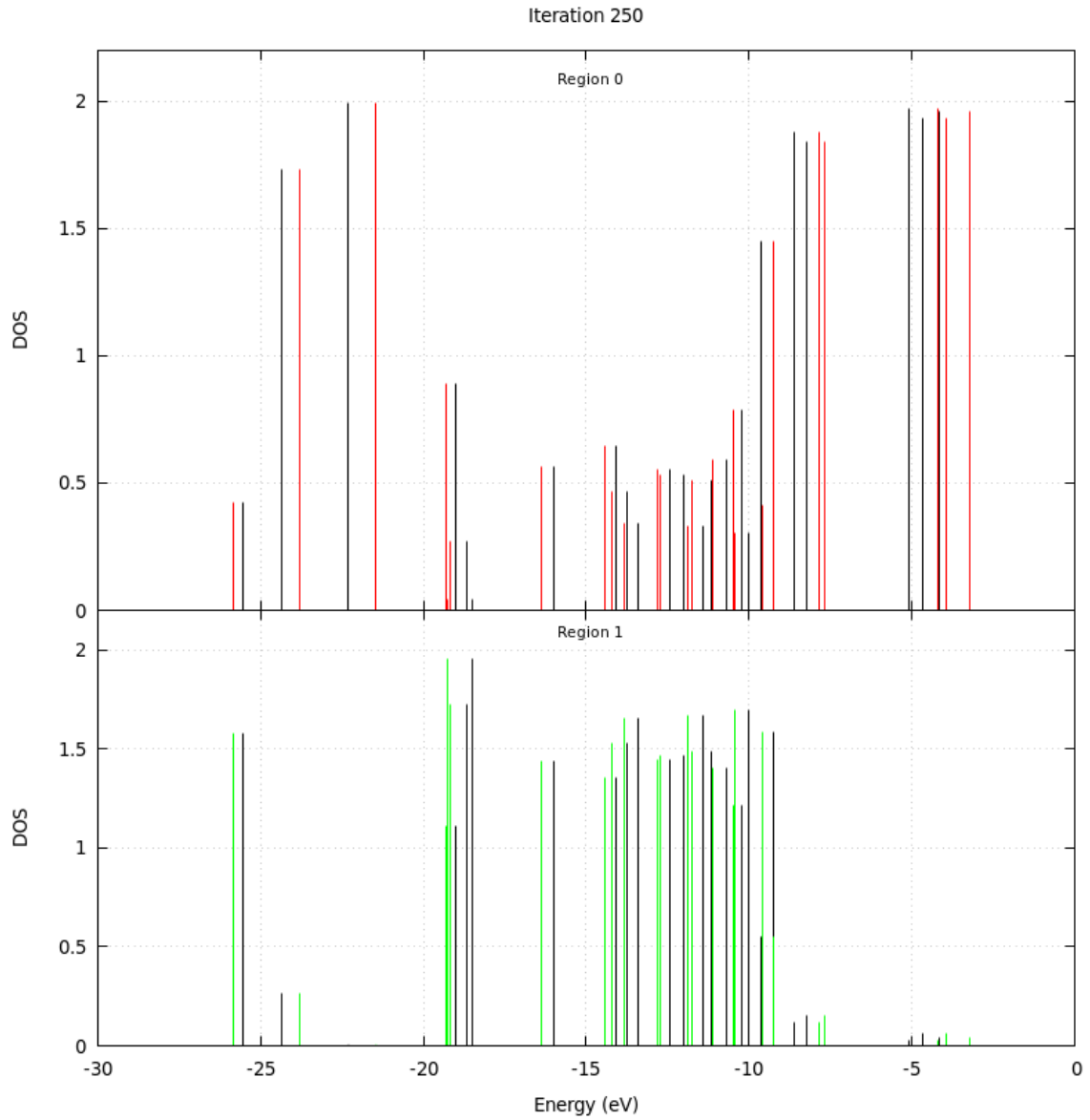


Figure B.1: Local density of states in the betaine molecule for iteration 250. For a detailed explanation of what is represented see figure 3.9.



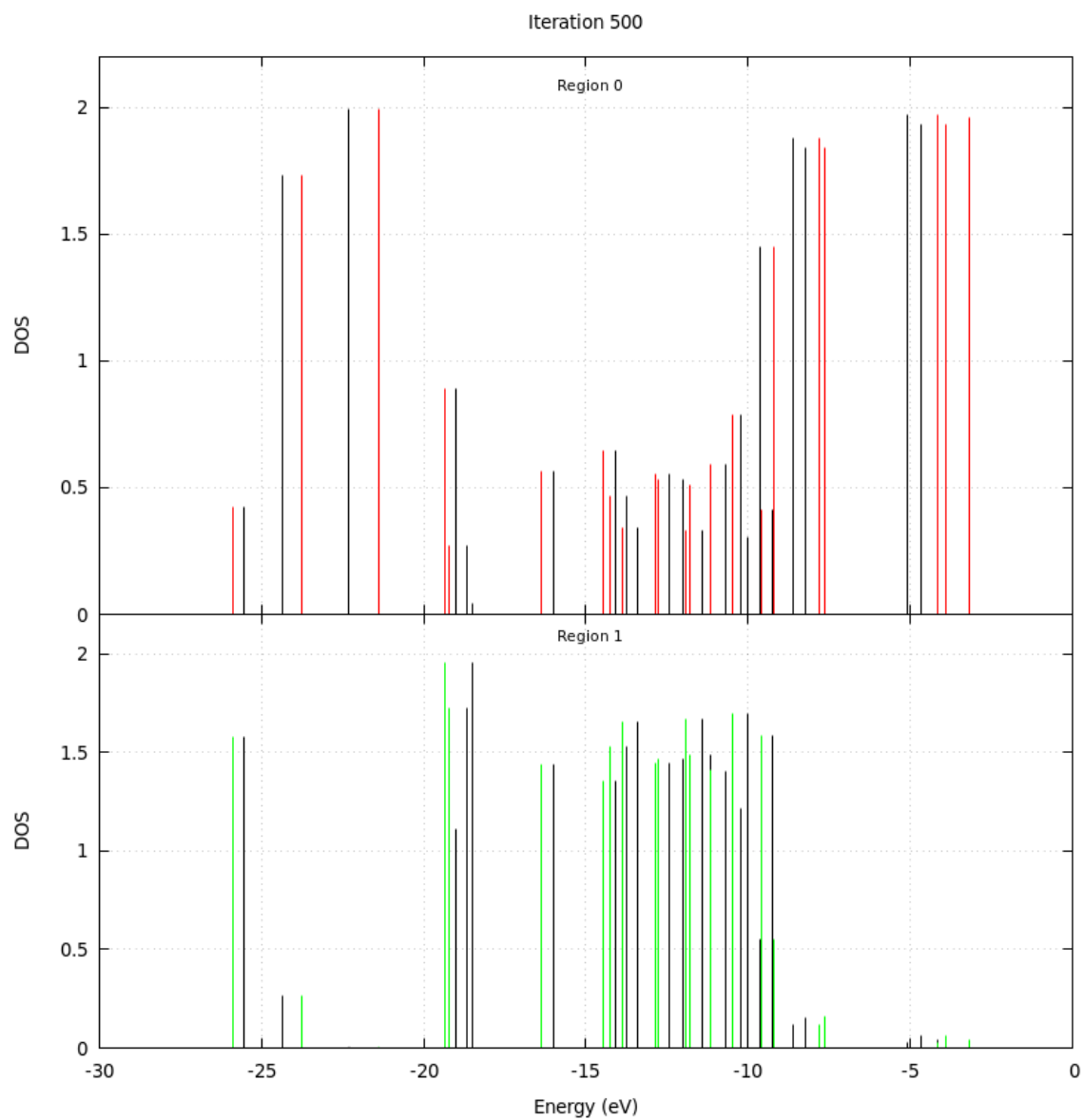


Figure B.2: Local density of states in the betaine molecule for iteration 500. For a detailed explanation of what is represented see figure 3.9.

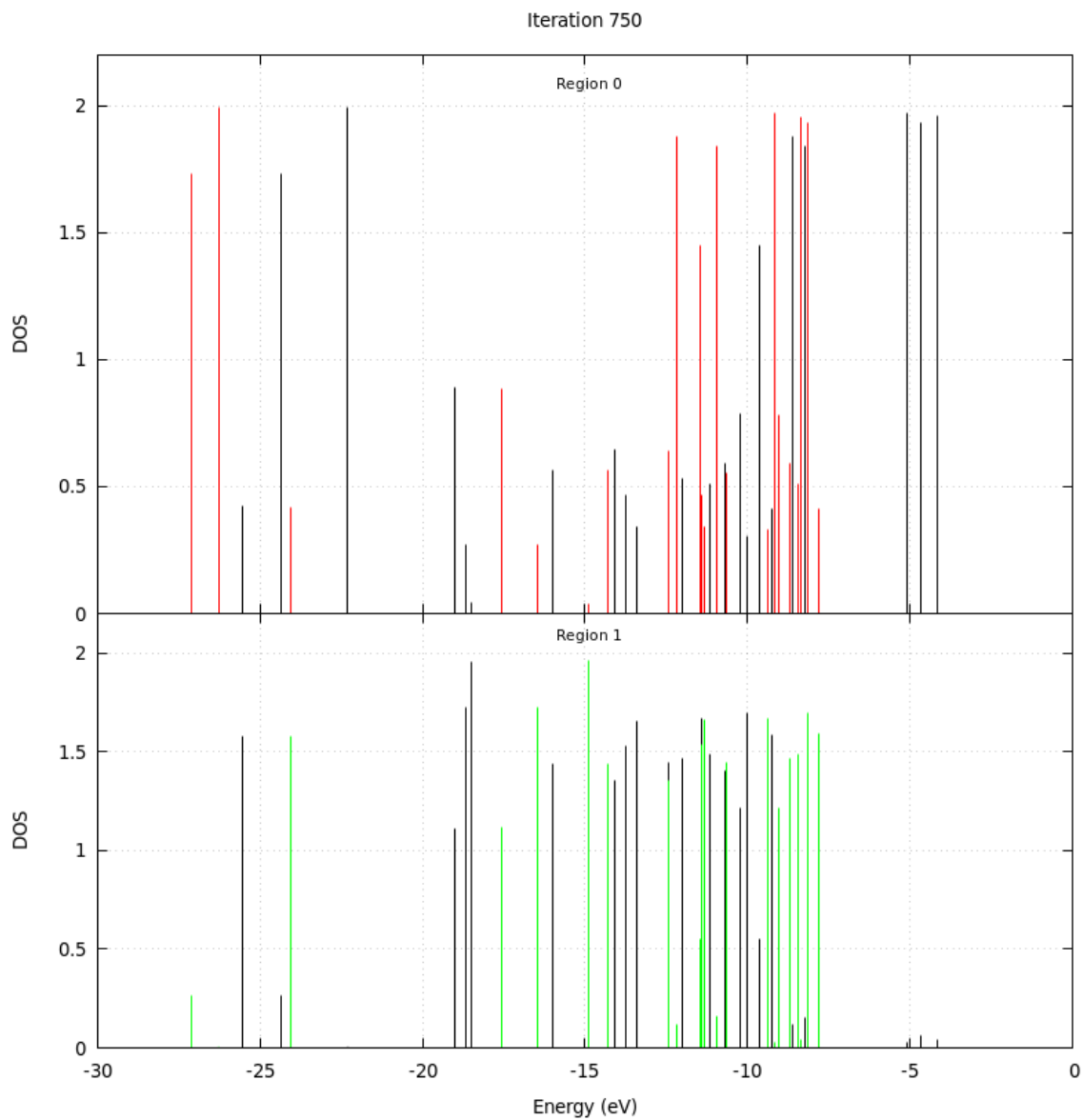


Figure B.3: Local density of states in the betaine molecule for iteration 750. For a detailed explanation of what is represented see figure 3.9.

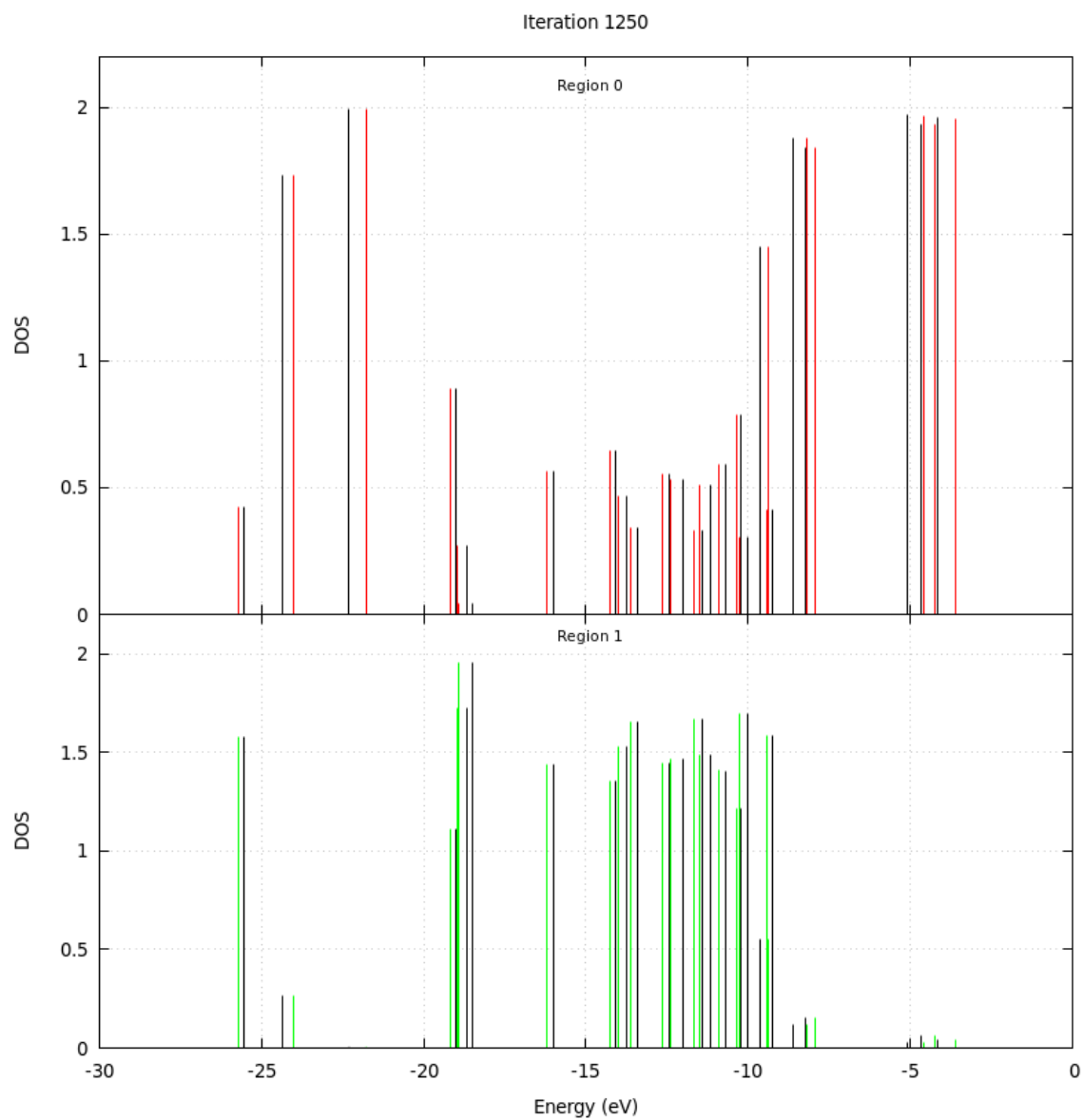


Figure B.4: Local density of states in the betaine molecule for iteration 1250. For a detailed explanation of what is represented see figure 3.9.

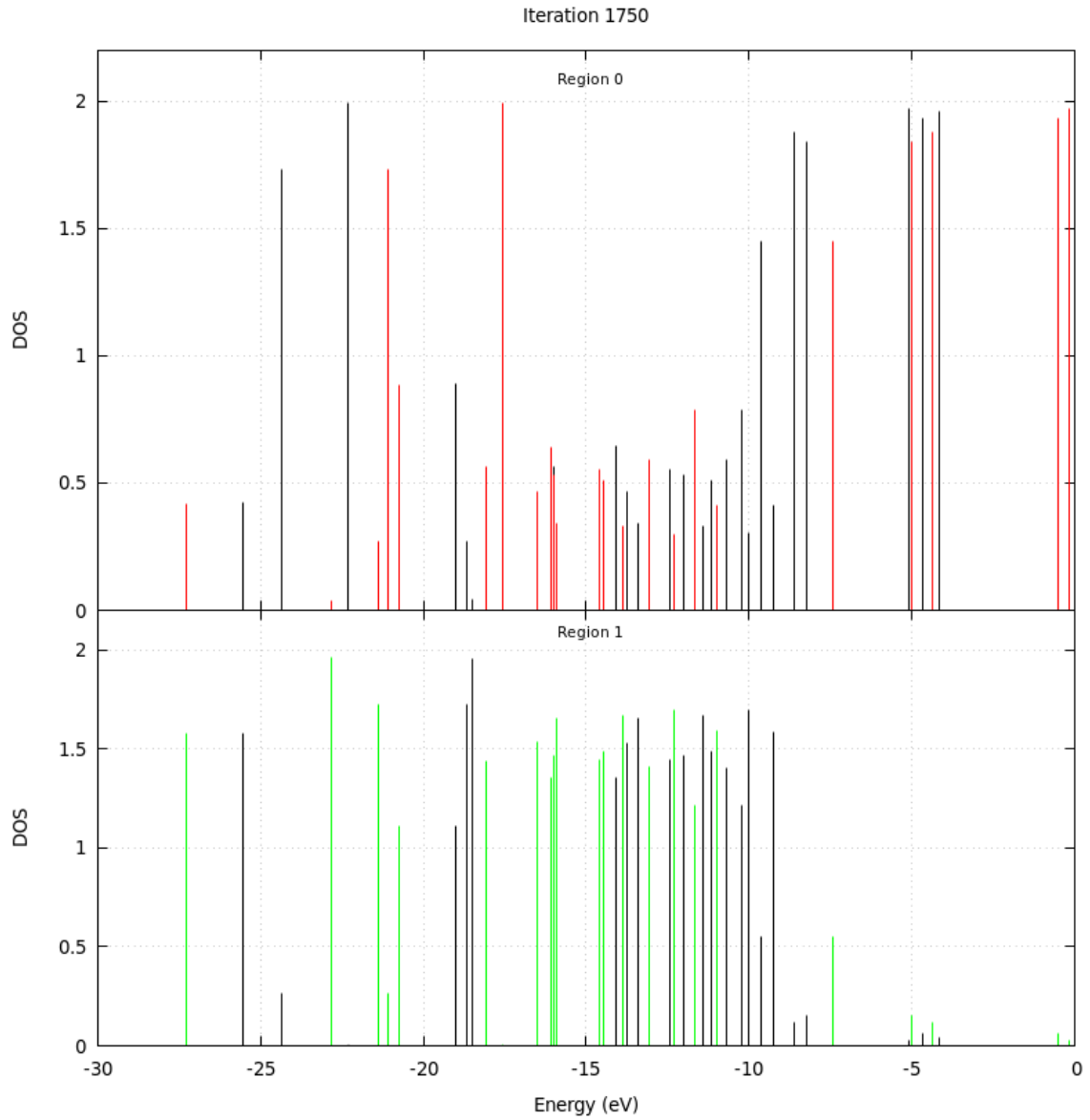


Figure B.5: Local density of states in the betaine molecule for iteration 1750. For a detailed explanation of what is represented see figure 3.9.

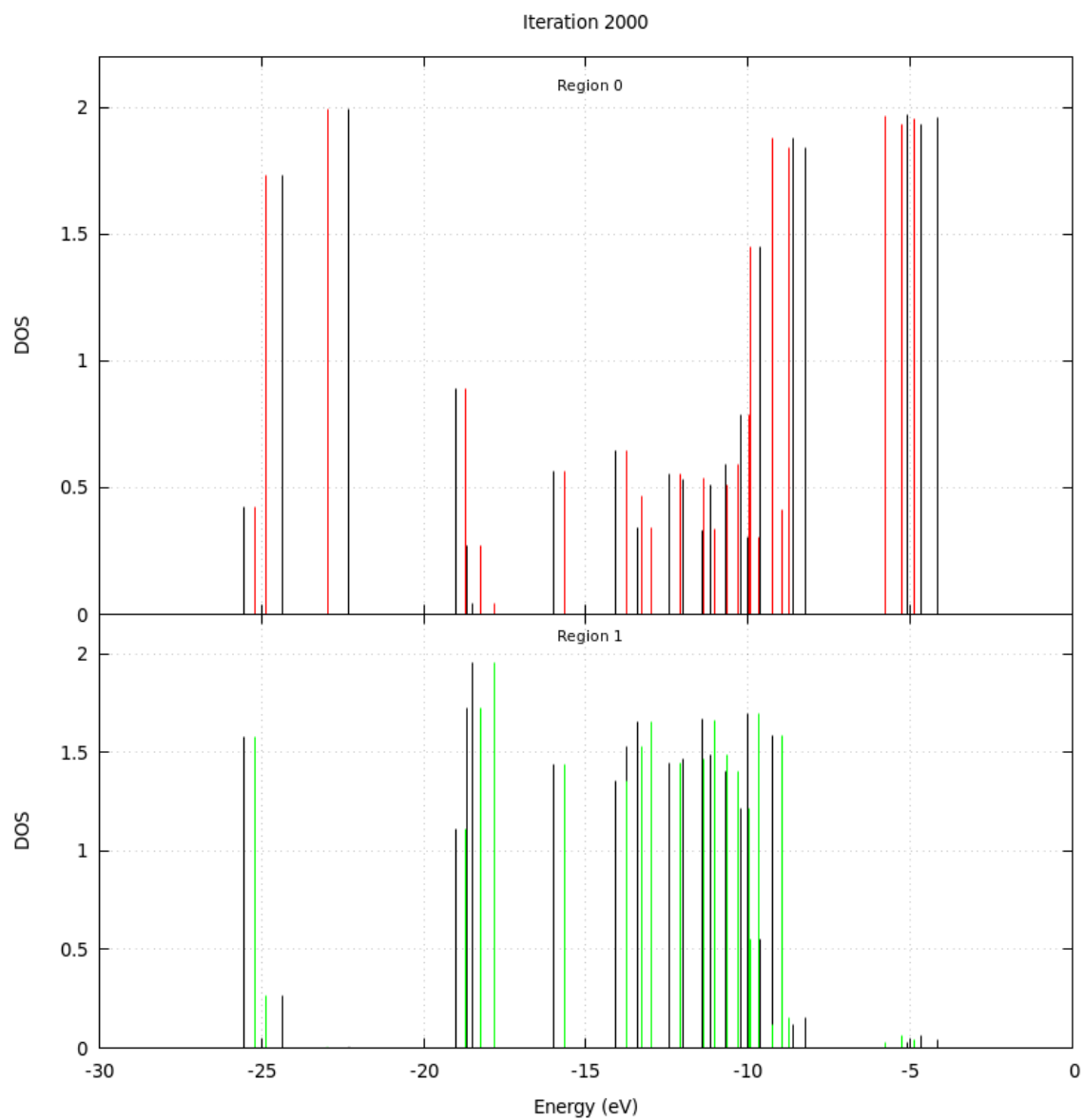


Figure B.6: Local density of states in the betaine molecule for iteration 2000. For a detailed explanation of what is represented see figure 3.9.

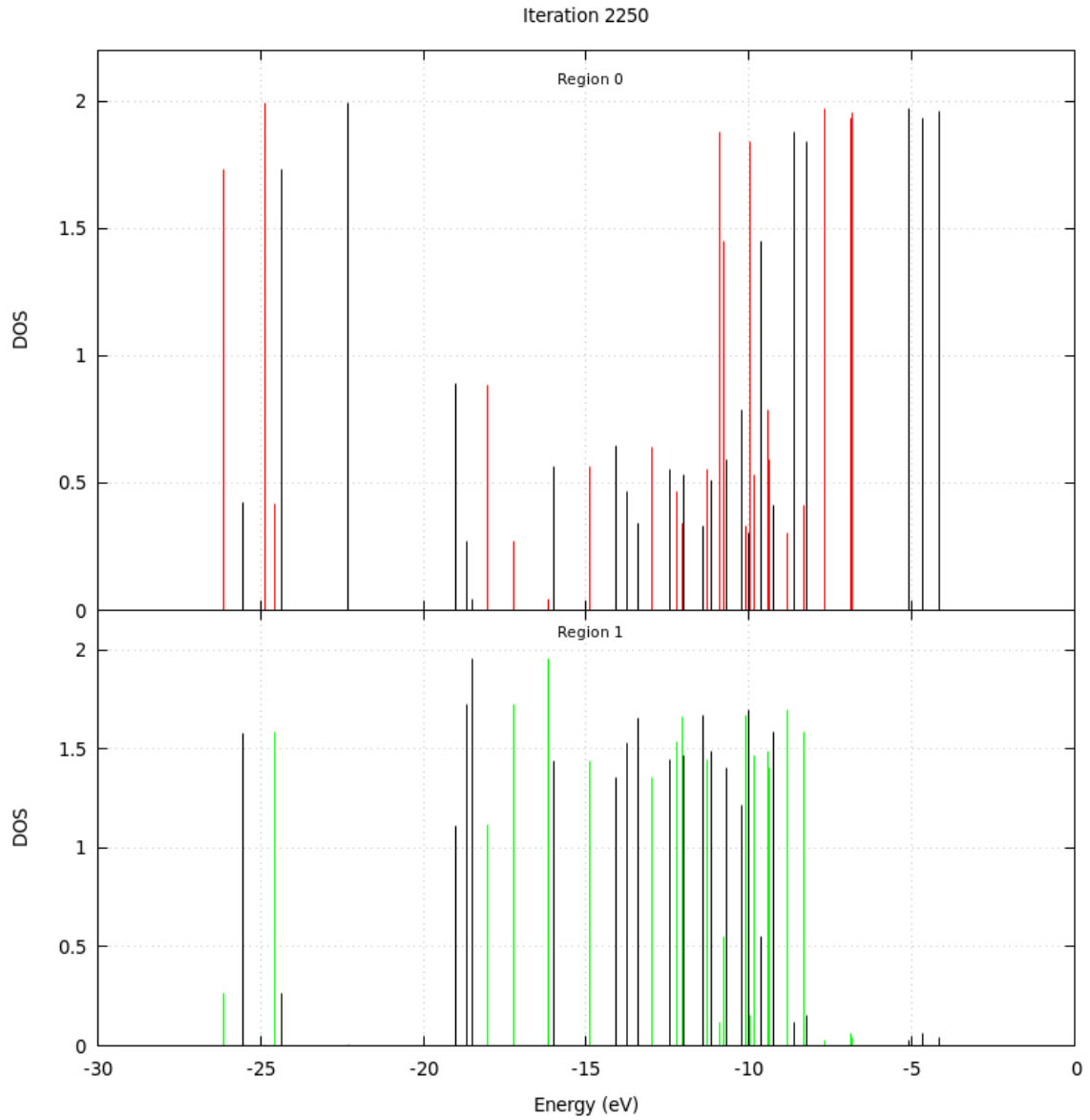


Figure B.7: Local density of states in the betaine molecule for iteration 2250. For a detailed explanation of what is represented see figure 3.9.

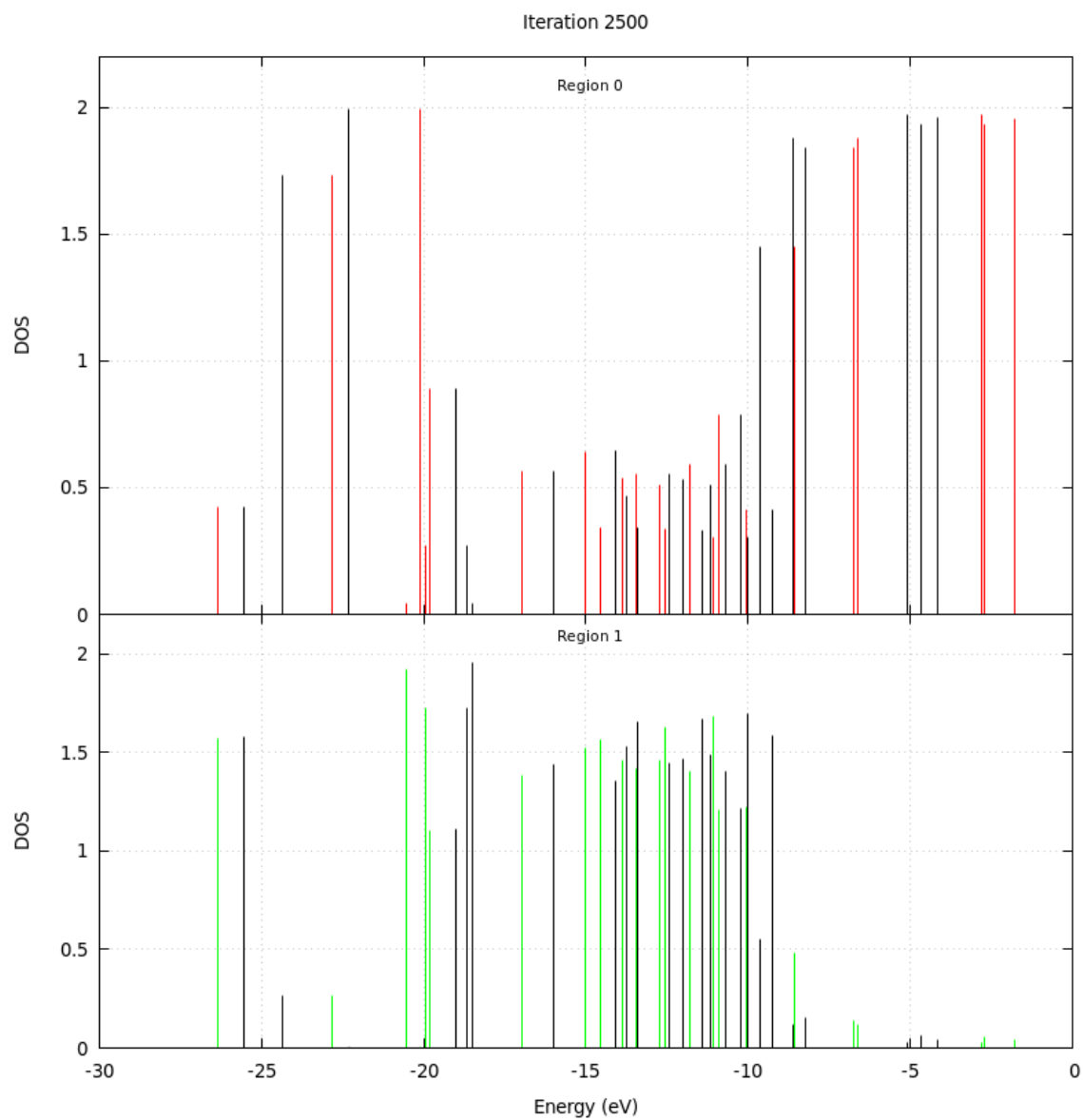


Figure B.8: Local density of states in the betaine molecule for iteration 2500. For a detailed explanation of what is represented see figure 3.9.

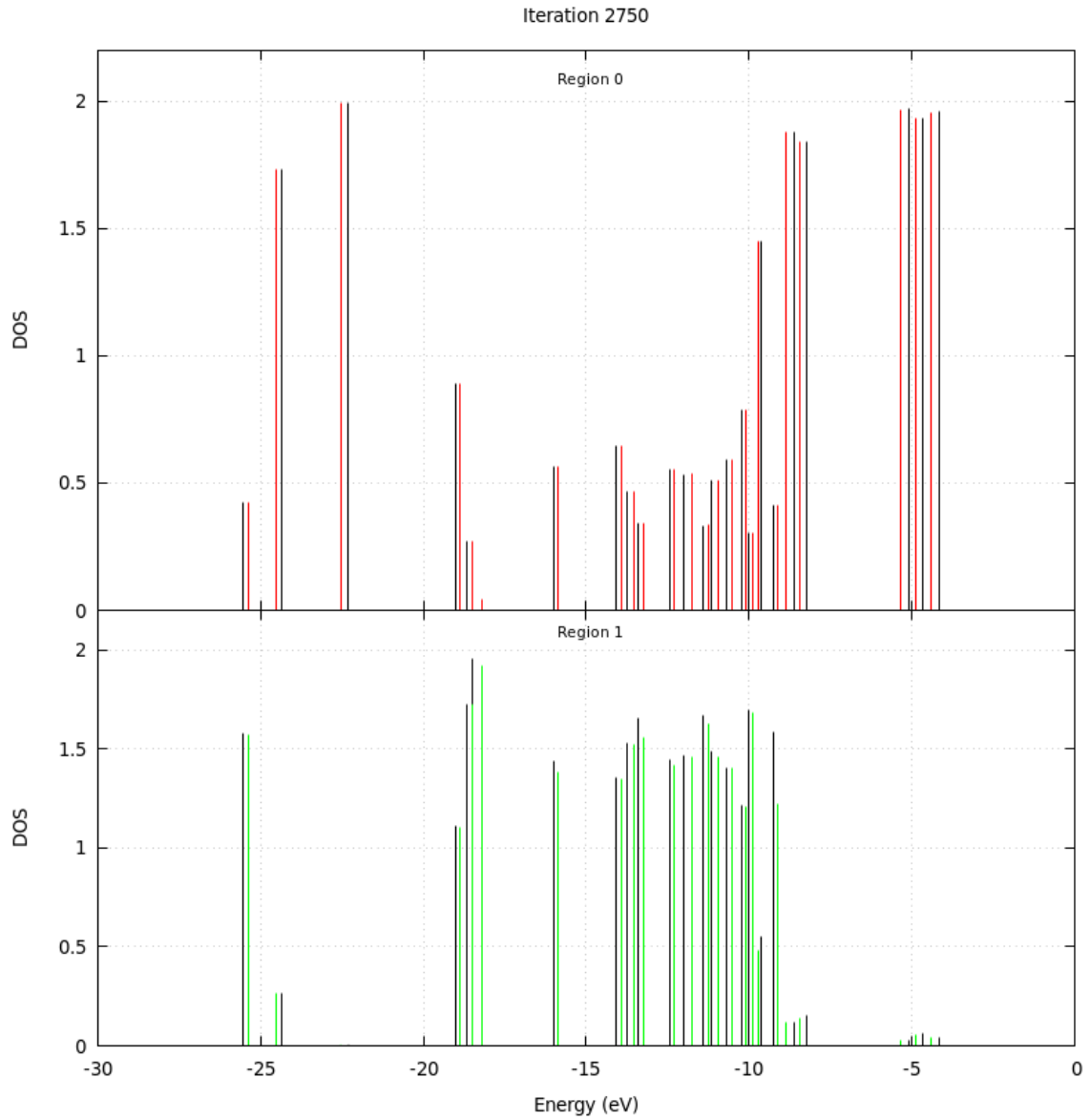


Figure B.9: Local density of states in the betaine molecule for iteration 2750. For a detailed explanation of what is represented see figure 3.9.



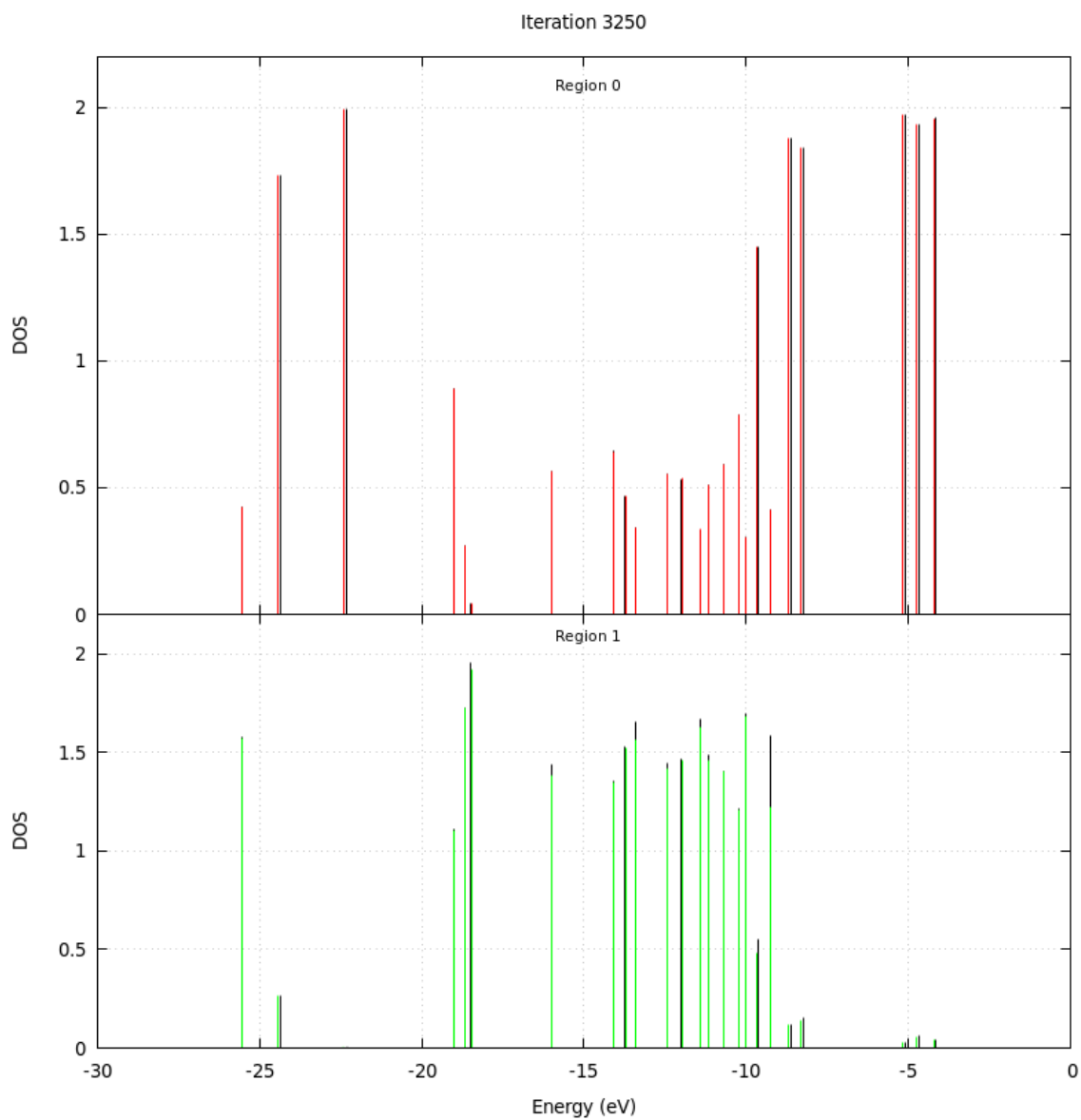


Figure B.10: Local density of states in the betaine molecule for iteration 3250. For a detailed explanation of what is represented see figure 3.9.

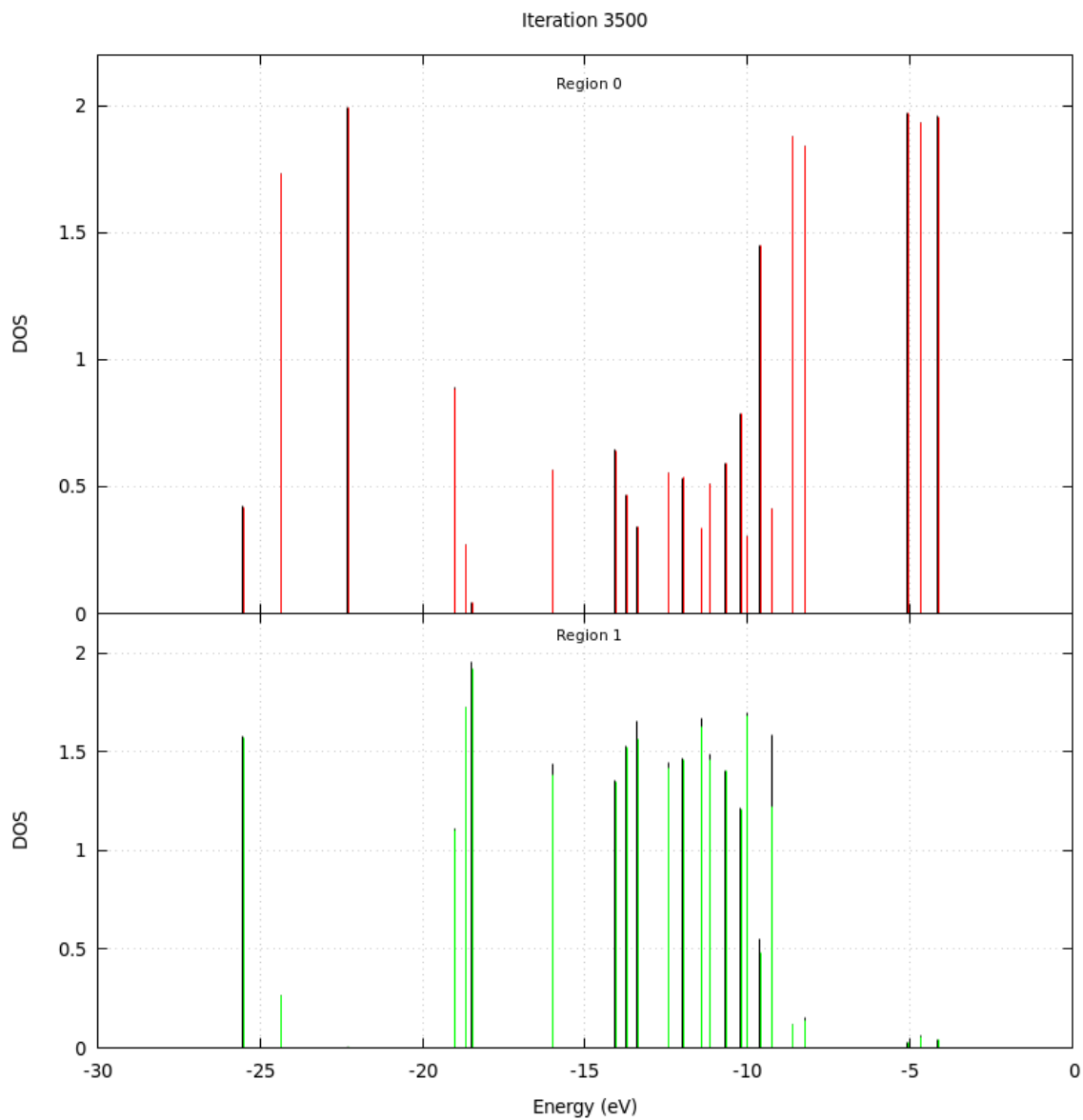


Figure B.11: Local density of states in the betaine molecule for iteration 3500. For a detailed explanation of what is represented see figure 3.9.

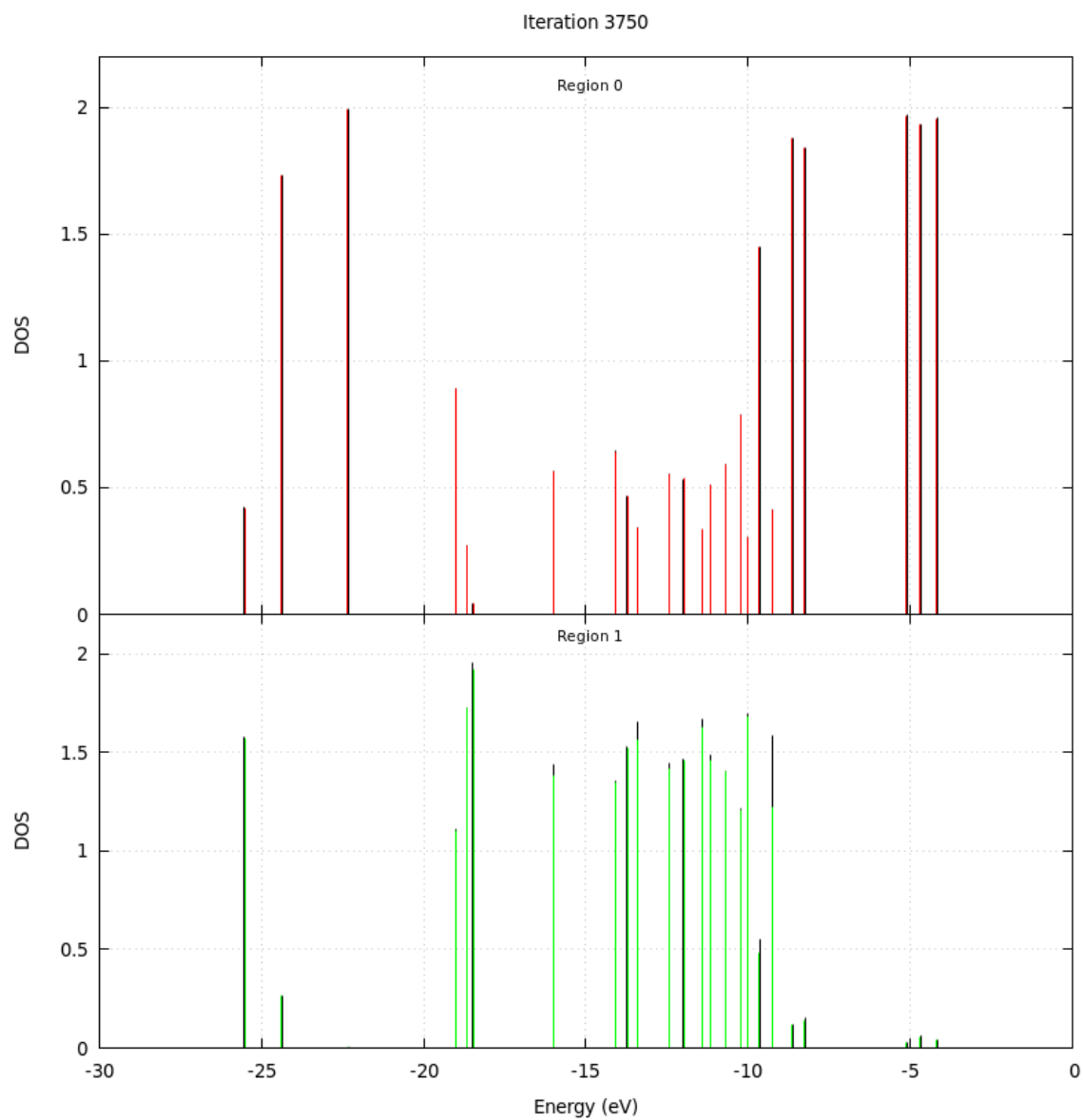


Figure B.12: Local density of states in the betaine molecule for iteration 3750. For a detailed explanation of what is represented see figure 3.9.

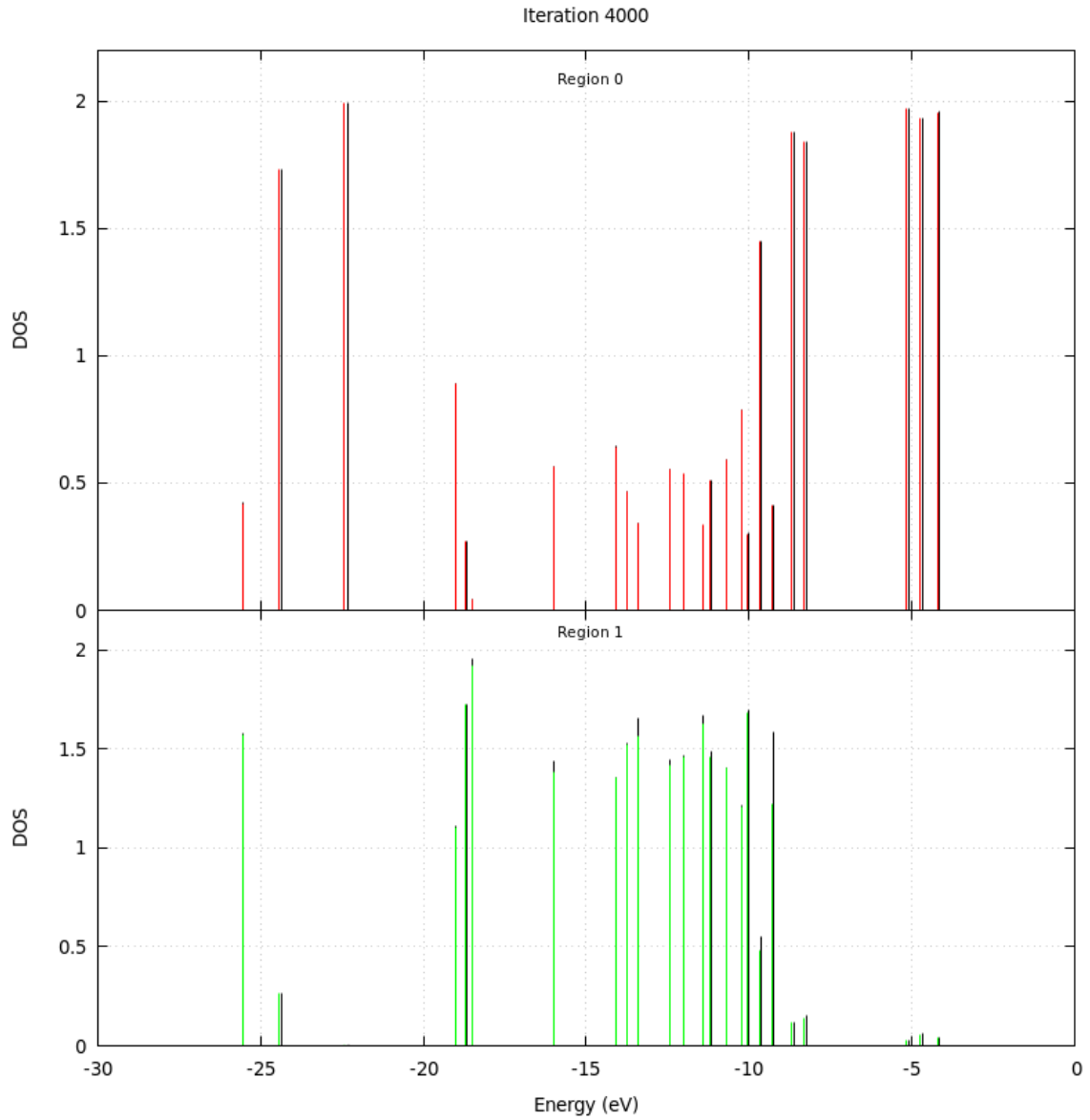


Figure B.13: Local density of states in the betaine molecule for iteration 4000. For a detailed explanation of what is represented see figure 3.9.

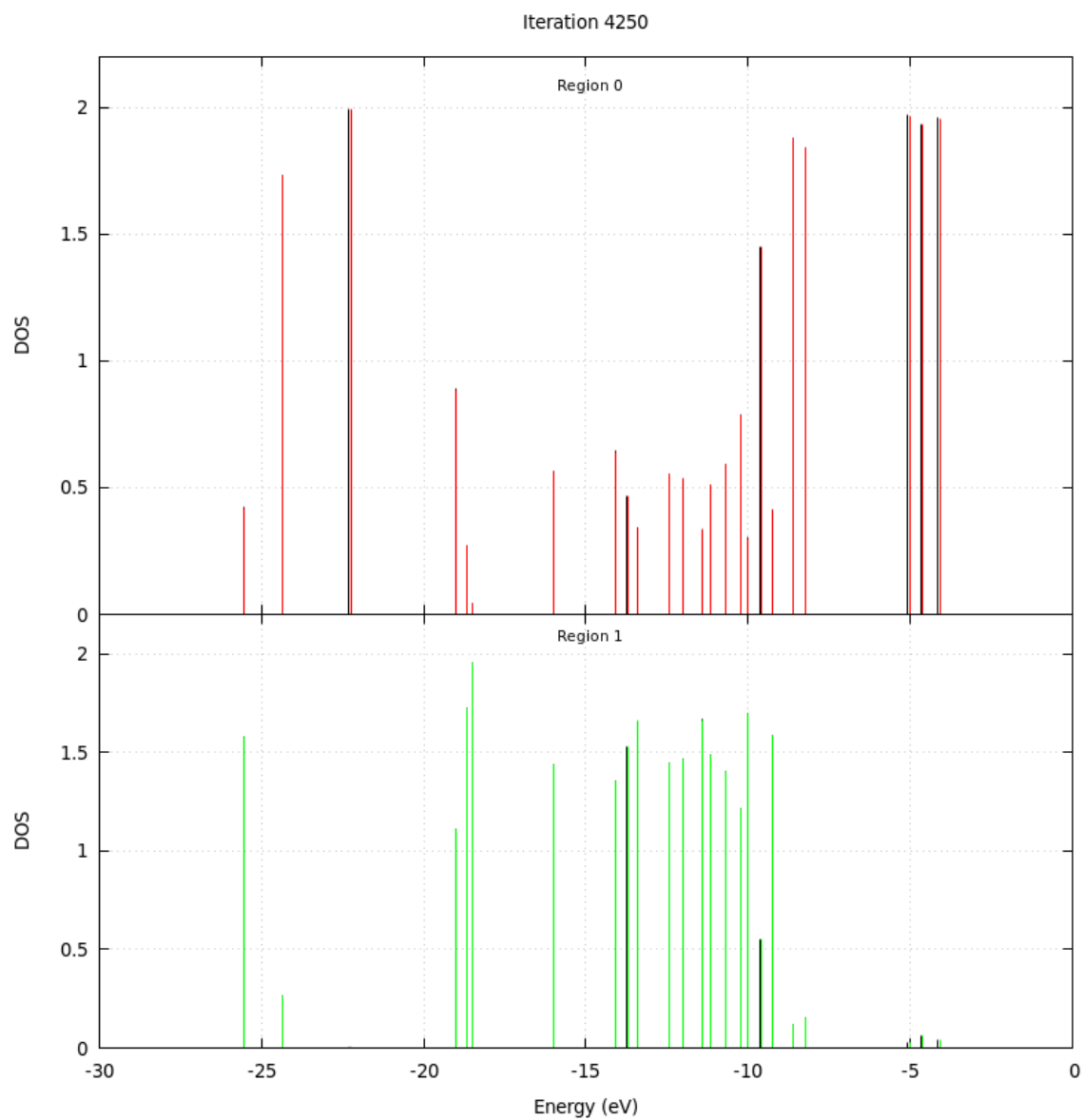


Figure B.14: Local density of states in the betaine molecule for iteration 4250. For a detailed explanation of what is represented see figure 3.9.

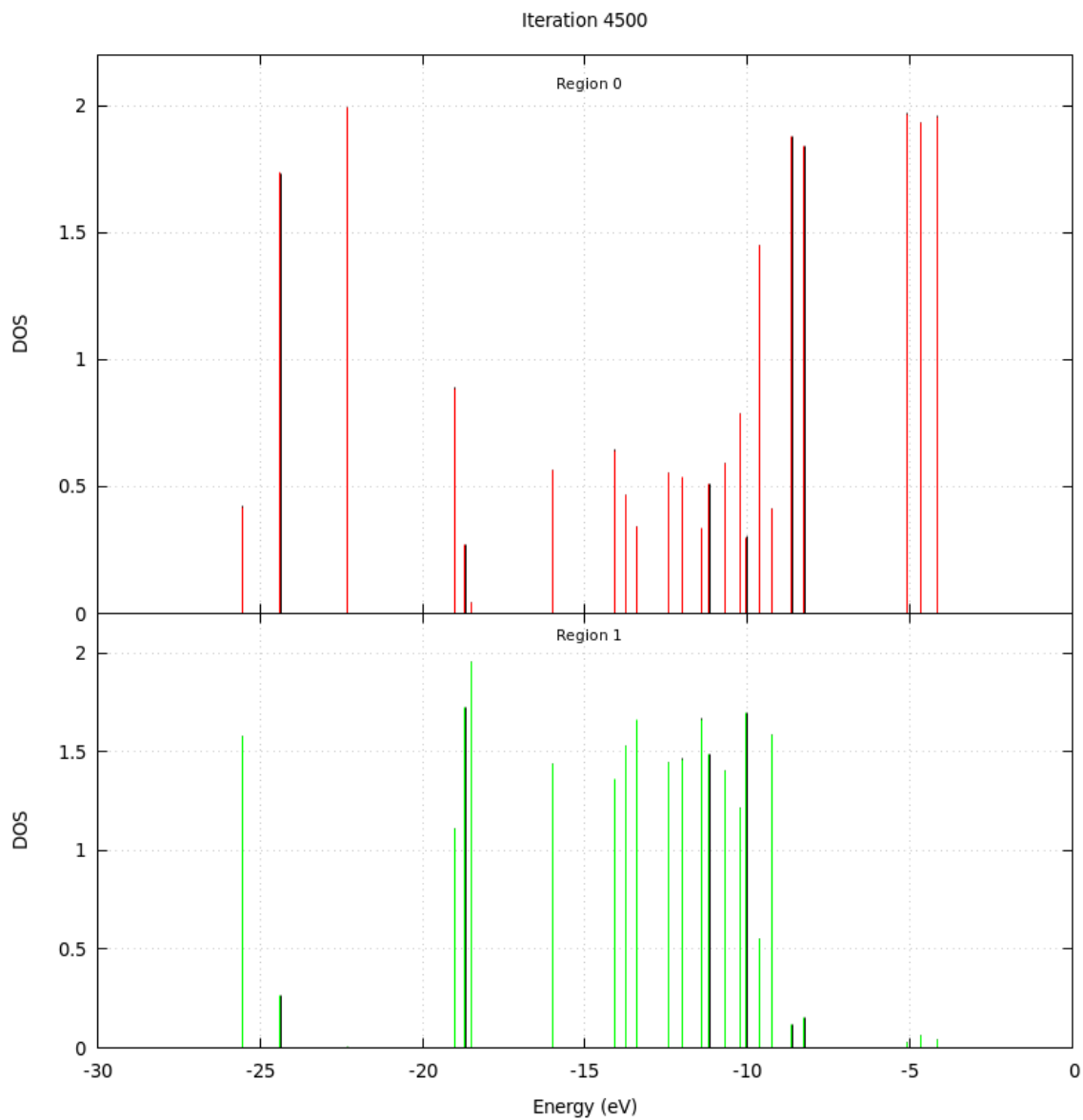


Figure B.15: Local density of states in the betaine molecule for iteration 4500. For a detailed explanation of what is represented see figure 3.9.

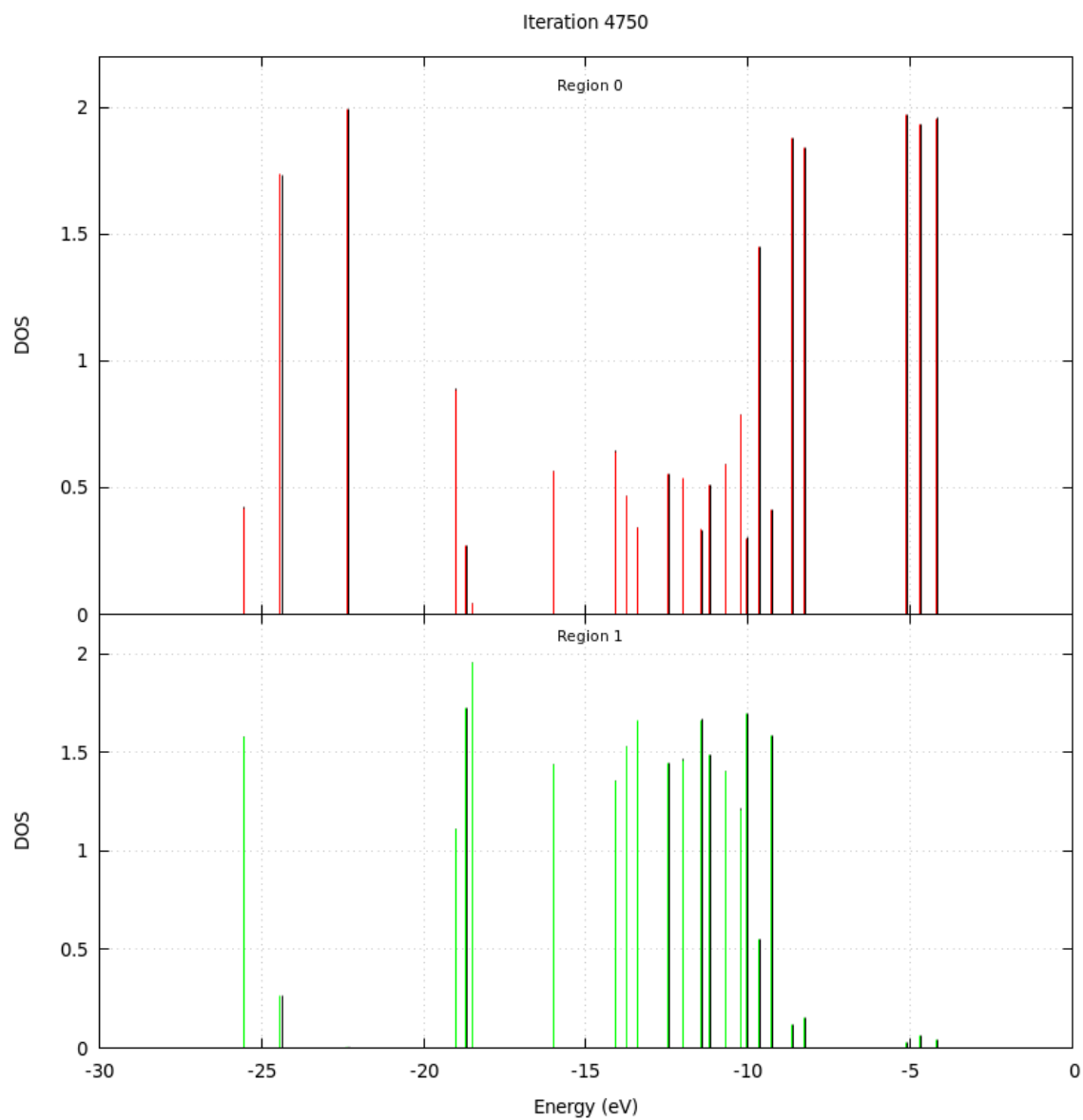


Figure B.16: Local density of states in the betaine molecule for iteration 4750. For a detailed explanation of what is represented see figure 3.9.

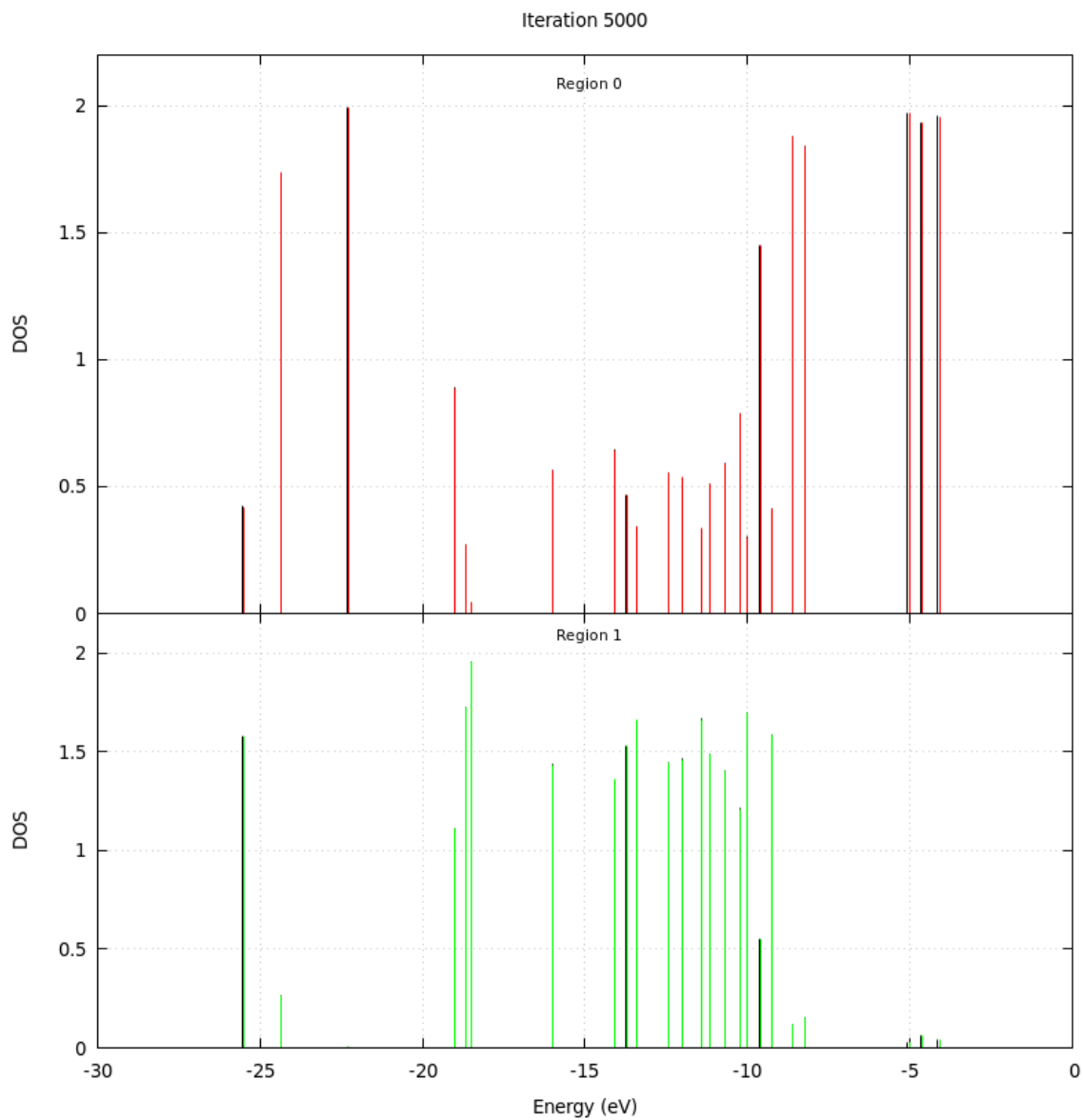


Figure B.17: Local density of states in the betaine molecule for iteration 5000. For a detailed explanation of what is represented see figure 3.9.



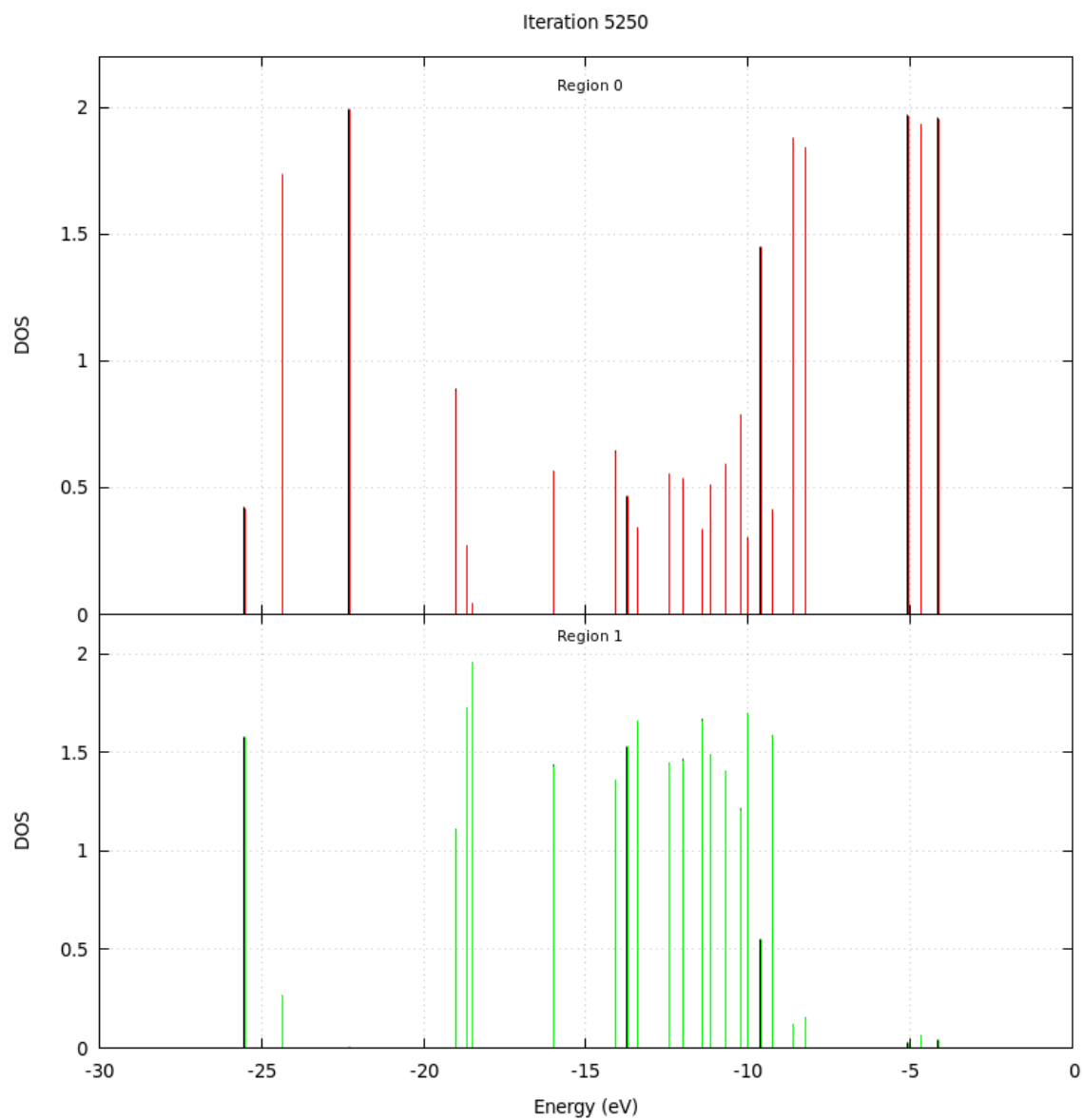


Figure B.18: Local density of states in the betaine molecule for iteration 5250. For a detailed explanation of what is represented see figure 3.9.

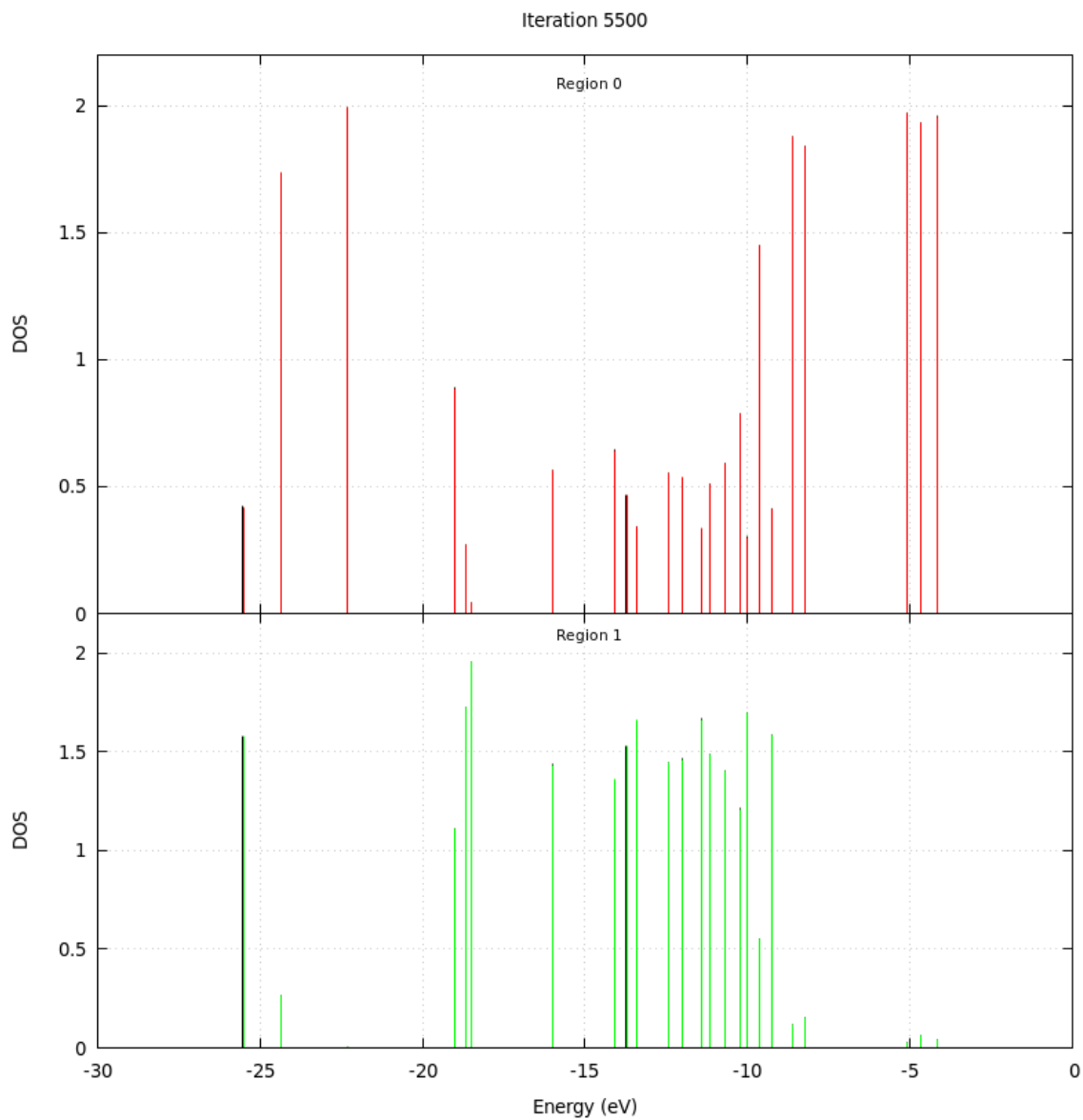


Figure B.19: Local density of states in the betaine molecule for iteration 5500. For a detailed explanation of what is represented see figure 3.9.

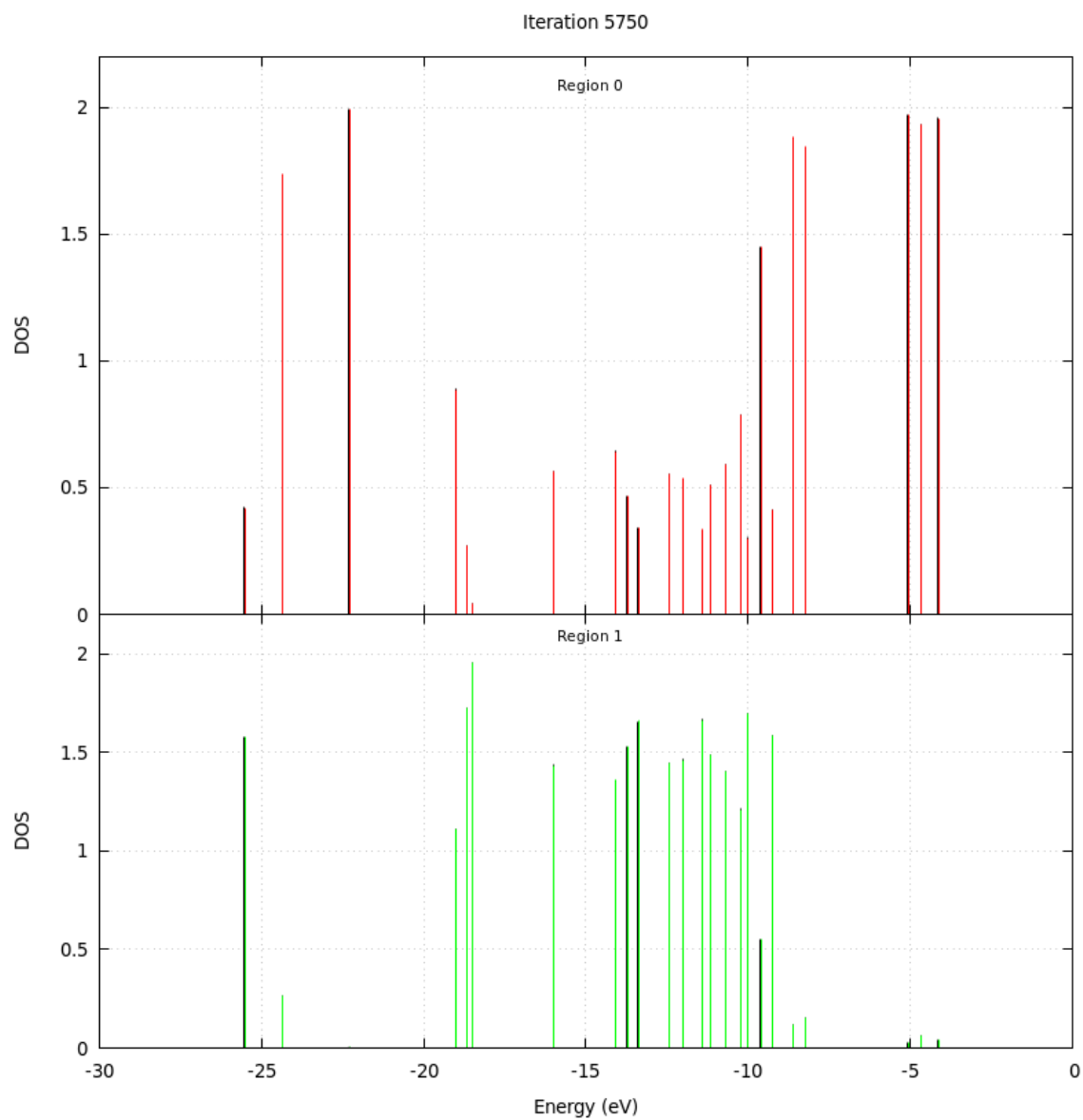


Figure B.20: Local density of states in the betaine molecule for iteration 5750. For a detailed explanation of what is represented see figure 3.9.

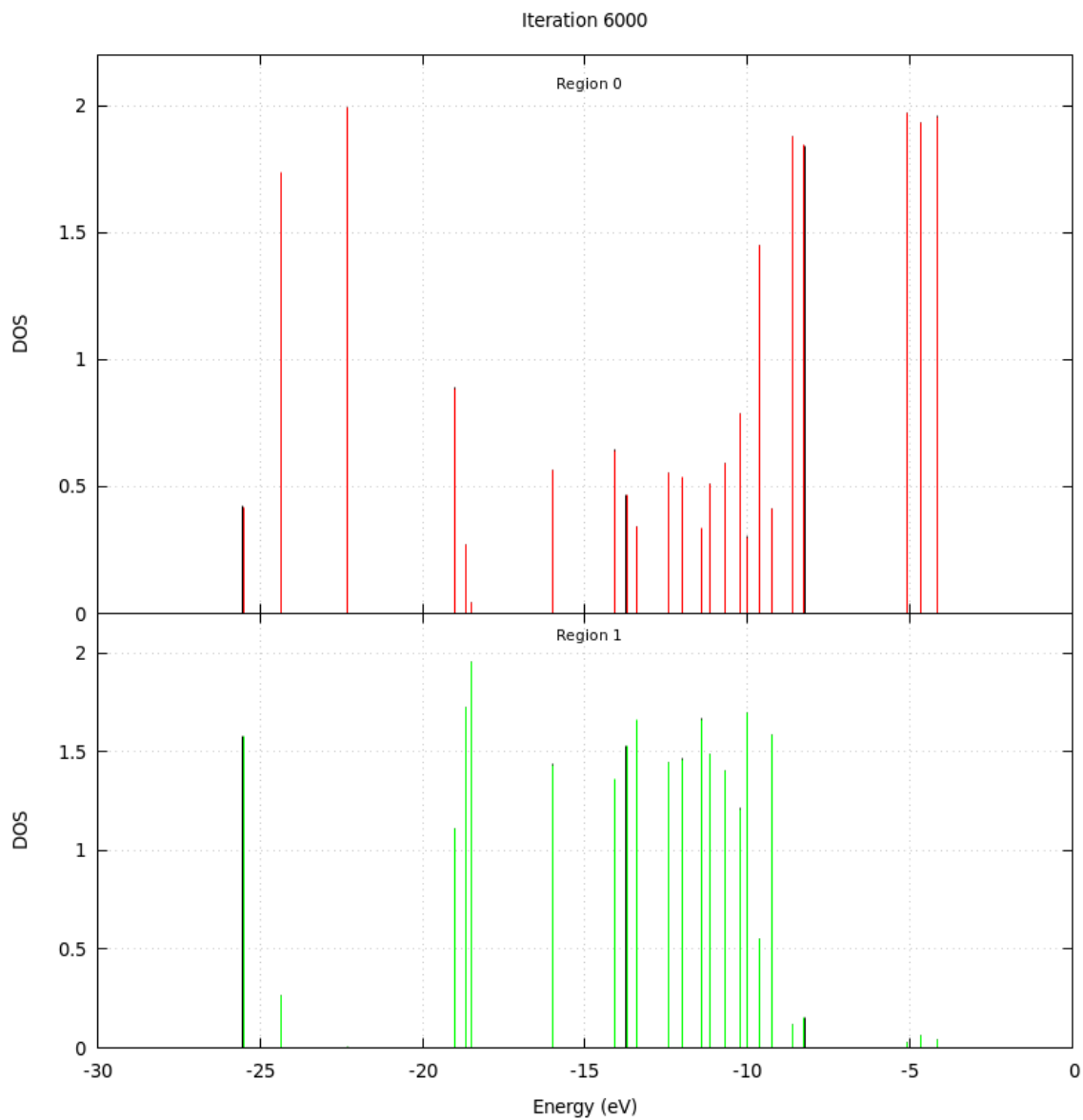


Figure B.21: Local density of states in the betaine molecule for iteration 6000. For a detailed explanation of what is represented see figure 3.9.